Quantifying Solute and Water Fluxes in Headwater Streams Using Passive Flux Meters

David P. Lee

Thesis submitted to the faculty of the Virginia Polytechnic Institute and State University in partial fulfillment of the requirements for the degree of

Master of Science
In
Forest Resources and Environmental Conservation

Kevin J. McGuire, chair
Brian D. Strahm
Daniel L. McLaughlin

May 8, 2018
Blacksburg, VA

Quantifying Solute and Water Fluxes in Headwater Streams Using Passive Flux Meters

David P. Lee

ABSTRACT

Passive samplers can be used to determine time-integrated patterns of water chemistry at one or many locations throughout a stream network while minimizing cost and sampling time. A passive flux meter (PFM) simultaneously estimates time-averaged water and solute mass fluxes in flowing water. PFMs have been used in groundwater to quantify contaminant flux but have been used only very recently in streams. In this study, PFMs were deployed in the surface and subsurface of headwater stream channels to examine the efficacy of the device to quantify mean concentrations of calcium, aluminum, and sulfur in streams of the Hubbard Brook Experimental Forest in New Hampshire, USA. In general, the PFM estimates of surface and subsurface stream chemistry were more accurate when flow rates were higher and more water passed through the PFM. During the lowest flows, PFMs overpredicted concentrations by 50 to 800%. In estimating calcium concentrations, 5 PFMs were within 10% of grab sample concentrations and 7 PFMs were within 30% of grab sample concentrations out of a total of 35 comparisons. Likewise, for sulfur concentrations, 4 PFMs were within 10% of grab sample concentrations and 7 PFMs were within 30% of grab sample concentrations out of 35 comparisons. Concentrations of aluminum were too low to be quantified above 90% confidence. PFMs calculated a lower cumulative discharge through the surface water PFMs than through the subsurface which may be explained by flow divergence around the sampler. Changes to PFM design and shorter deployment times are proposed to increase the efficacy of the PFM.

Quantifying Solute and Water Fluxes in Headwater Streams Using Passive Flux Meters

David P. Lee

GENERAL AUDIENCE ABSTRACT

Passive sampling of headwater streams has advantages over traditional water sampling in quantifying stream water chemistry over time and space, while minimizing cost and sampling time. A passive flux meter (PFM) is a sampler that estimates local time-averaged discharge of water and time-averaged solute amount in flowing water without the need for constant monitoring, maintenance, or power sources. PFMs have been used in groundwater systems to quantify contaminant concentrations but have only been used very recently in streams or in the sediments below streams. In this study, PFMs were installed in headwater streams and the shallow sediments below the streams to examine the ability of the device to quantify the natural water chemistry. Concentrations of calcium, aluminum, and sulfate were evaluated in streams of the Hubbard Brook watershed in New Hampshire, USA. Concentrations of aluminum were too low to be quantified. In general, the PFM estimates of surface and subsurface stream chemistry were more accurate when flow rates were higher and more water passed through the PFM. During the lowest flows, PFMs overestimated stream concentrations. PFMs installed in small streams measured more total volume through the device than PFMs installed in sediments below the streams. PFM design may have had an impact on these results. Changes to PFM design and shorter deployment times are proposed to increase the efficacy of the PFM.

Acknowledgements

I would first like to thank my advisor, **Kevin McGuire**, for unrelenting support and motivation in my tenure as a graduate student. He challenged me throughout every step of my project to think independently and be self-motivated. I am incredibly grateful for his unwavering support of my work and his ability to guide me in my relentless quest to gain more knowledge about the world and its natural resources.

I would also like to thank **Scott Bailey** for his support and friendship. Scott was my field advisor at the Hubbard Brook Experimental Forest, served on my committee for a most of my program, and provided countless insights and pieces of advice regarding my project. Scott provided innumerable data files and many hours of planning and sampling. His guidance and knowledge of Hubbard Brook helped me have a successful field season.

I would like to thank **Daniel McLaughlin** and **Brian Strahm** for serving on my committee. I have Daniel to thank for providing the spark that led me to change career paths, motivating me to pursue a Master's degree at Virginia Tech, as well as challenging me to see the bigger picture in every scenario. I will always appreciate the support he has shown me over the years. I would like to thank Brian for providing unending aid in my data analysis efforts, and his knowledge of soil chemistry, laboratory analysis protocols, and uncertainty has aided me more times than I can count.

A special thanks to **Mehdi Ashraf-Khorassani** for taking many hours out of his time to help me develop the GC-FID protocol for analyzing alcohol samples. Without him, I would not have been able to succeed in the laboratory.

In addition, everyone at Virginia Tech that made my time there special deserves a special thank you: **Andrés Peralta-Tapia** for his help in my field work and lasting friendship, **Dave Mitchem, Athena Tilley,** and **Stephanie Duston** for their lab help, **Inga Solberg** for her guidance at the Virginia Water Resources Research Center, and **Kyle Strom** for his many conversations on open channel hydraulics and flow divergence.

At Hubbard Brook, many people deserve thanks from me for their support during my field season and beyond. Thanks to **Geoff Wilson, Tammy Wooster, Amey Bailey, Ian Halm, Don Mower, Hannah Vollmer, Gabe Winant, Todd Dickinson, Mark Green, Zoë Klein,** and **Leonie Kiewiet**.

Table of Contents

List of Tables

List of Figures

List of Abbreviations / Symbols

C_D	Drag coefficient of a device in a stream [–]
C_i	Initial tracer concentration in granular activated carbon sample $\left[\frac{mg}{L}\right]$
C_f	Final tracer concentration in granular activated carbon sample $\left[\frac{mg}{L}\right]$
CPVC	Chlorinated polyvinyl chloride
Da	Darcy number; measure of permeability in a porous media
DC	Deployment control PFM
DMP	2-4-dimethyl-3-pentanol
EtOH	ethanol
GC-FID	Gas Chromatograph with Flame Ionization Detector
HCl	Hydrochloric acid
IBOH	isobutanol
KCl	Potassium chloride
K_D	Partitioning coefficient of tracer on GAC $\left[\frac{mL}{g}\right]$
MeOH	methanol
M_R	Relative mass of tracer remaining on PFM after deployment [–]
IPA	isopropyl alcohol
GAC	granular activated carbon
PVC	Polyvinyl chloride
q_x	Water flux through the PFM – flow per unit cross sectional area $\left[\frac{m}{s}\right]$
R_D	Retardation factor; ratio of velocity of water through GAC to velocity of tracer through GAC [–]
Re	Reynolds number of stream; measure of degree of flow turbulence [–]
Re_D	Reynolds number of water through the device [–]
tBA	tert-butyl alcohol
TC	Transport control PFM
V_{iso}	volume of isobutanol extractant in granular activated carbon sample $[L]$
W3	Watershed 3 at the Hubbard Brook Experimental Forest
W9	Watershed 9 at the Hubbard Brook Experimental Forest

ZZ	Zig Zag Brook watershed at the Hubbard Brook Experimental Forest
η	Interception efficiency of a porous cylinder – ratio of flow through cylinder to flow around the cylinder
ρ_B	Bulk density of granular activated carbon $\left[\frac{g}{mL}\right]$
θ	Porosity of granular activated carbon [–]
ξ	Pore volume of water associated with flux through granular activated carbon in column test [–]

Chapter One

1.0. Introduction

1.1. Problem context

Forested headwater streams are important sources of water for downstream ecosystems and water supply for human communities (Lowe et al. 2005, Benstead et al. 2012, Acuña et al. 2014, Wohl 2017). Headwater streams, defined here as 1st and 2nd order streams, are known to dampen downstream flood pulses, cycle nutrients, and set water quality for downstream aquatic ecosystems (Bernhardt et al. 2003, Klaminder et al. 2006, Sanford et al. 2007). Management practices and land use in forested headwater catchments can influence water quantity and quality and can thus impact these important stream ecosystems. Headwater streams have been shown to be areas where land management strategies have the greatest effect on downstream water quality (Alexander et al. 2007, Bryant et al. 2007, Dodds et al. 2008). As such headwater streams are significant contributors to downstream ecosystems and vulnerable to changes in land use and management.

In addition to their functional importance, headwater streams dominate global stream length, as over 75% of global stream length can be attributed to 1st and 2nd order streams (Downing et al. 2012, Wohl 2017). In addition, the length of perennial and temporary headwater streams is often underestimated (Bishop et al. 2008, Benstead et al. 2012, Elmore et al. 2013, Fritz et al. 2013). For example, remote sensing revealed that total perennial stream length was double that of previous estimates in a Swedish study, and that over 90% of the national perennial stream length had catchment areas under 15 km^2 (Bishop et al. 2008).

Given their spatial extent, valued functions, and vulnerability, the characterization of headwater streams and their chemical and physical processes is critical to furthered understanding and protection of these important systems. However, a major challenge exists in monitoring

headwater stream systems. These streams can be relatively inaccessible, poorly inventoried, and infrequently sampled. Passive sampling methods can be a solution to characterizing the chemical water quality of these systems, as they can be left at specific sites to capture time-averaged representations of discharge and chemistry.

1.2. Background

1.2.1. Characterizing chemical variability in headwater streams

Forest headwater stream chemistry variation is driven by processes at multiple spatial and temporal scales (Temnerud et al. 2005, Tiwari et al. 2017, Abbott et al. 2018). Water chemistry can rapidly change over time and throughout the stream network challenging accurate characterization and the understanding of processes that drive chemical concentrations and loads in streams. Even in well-studied research catchments, drivers of stream chemistry and their resulting effects on spatial and temporal chemical patterns are difficult to quantify. Topography, land use, geologic structure, soil, in-stream processing, and groundwater inputs are drivers that have been shown to influence the chemistry of headwater streams (Johnson et al. 2000, Clinton et al. 2006, Bailey et al. 2014, McGuire et al. 2014, Musolff et al. 2015). However, quantifying the importance of these drivers on the chemical spatiotemporal variation is difficult often due to the lack of observations at appropriate temporal and spatial scales across environmental gradients.

Sampling stream water is typically limited to either high-frequency sampling at a point in space or multiple locations over larger areas at one point in time (Krause et al. 2015). Depending on sampling frequency and resources available, it is possible to miss important portions of the streamflow regime when solute transport is a dominant factor controlling stream chemical composition. Kirchner et al. (2004) demonstrated that chemical measurements taken weekly fail to reflect the close ties between hydrological and chemical dynamics in a watershed, including

during short-term events such as storms. Even daily chemical samples from headwater streams can conceal the immediate chemical responses of watersheds to storm events (Neal et al. 2012, Rode et al. 2016). However, new technologies including high-frequency sensors and in-line samplers expand the temporal resolution at which we can measure a suite of solutes and have shown greater chemical variation than previously thought existed (Crawford et al. 2015). However, resource constraints limit monitoring efforts as these approaches can be expensive and are typically used in one place. Thus, high frequency sensors at a specific location can fail to capture the "hot spots" of increased chemical reactivity that exist within a stream network (Krause et al. 2015). Further, the chemostatic behavior of many streams suggests the need to couple estimates of discharge and chemistry over time to adequately address mass flux estimations or determine representative flow-weighted concentrations (Godsey et al. 2009, Creed et al. 2015, Hunsaker et al. 2017).

It can be impractical to rely primarily on traditional water quality sampling techniques to characterize how stream chemistry and discharge vary in space and across different time scales. Fixed point auto-sampling and high-frequency sensors are expensive and require significant labor with data collection and data analysis (Padowski et al. 2009, Rozemeijer et al. 2010). Thus, new passive sampling methods have been developed to provide cost-effective flow-weighted solute concentration data across multiple locations (Klammler et al. 2007, Padowski et al. 2009).

1.2.2. Passive flux meter use in water quality monitoring

Passive samplers have the potential to resolve issues that arise when characterizing the spatial and temporal variability of streams. First, they avoid some of the challenges associated with solute export estimation using grab samples and discharge measurements (Johnson 1979, Swistock et al. 1997) by determining a time-integrated or flow-weighted average estimation of chemistry (Rozemeijer et al. 2010). They are also relatively inexpensive to make and therefore can be

deployed throughout a watershed to observe chemical variation at multiple points throughout a stream network (Padowski et al. 2009). Passive flux meters (PFMs) are relatively new passive samplers that use an integrative sampling technique to characterize the chemical composition of streams and groundwater (Annable et al. 2005, Padowski et al. 2009). PFMs combine the measurement of cumulative solute mass load and water flux through the sampler, for determining flow-weighted concentration or average velocities and concentration over a deployment period (Klammler et al. 2007). PFMs were first developed for estimating contaminant transport in groundwater (Hatfield et al. 2004, Annable et al. 2005, Basu et al. 2006, Verreydt et al. 2013). Prior deployments of PFMs have been in groundwater contaminated with chlorinated solvents (Annable et al. 2005). However, recent use of PFMs has been expanded to applications in stream water and in the hyporheic zone (Klammler et al. 2007, Padowski et al. 2009, Kunz et al. 2017). Further, the use of PFMs in streams has been mainly limited to field sites known to exhibit relatively stable and high concentrations of nitrogen and phosphorus and stable flow (Klammler et al. 2007, Padowski et al. 2009). Padowski et al. (2009) showed that water flux from their PFM was within 3% of water flux calculated with standard velocity and area measurements and phosphate flux from their PFM was within 7% of phosphate flux calculated using grab sample concentrations and water flux estimates. The few PFM studies conducted in streams were in nutrient-rich, low-gradient streams; therefore, more work is needed to examine their applicability in streams of varying velocity and chemical composition (Klammler et al. 2007, Padowski et al. 2009). Furthermore, testing PFMs in systems with low solute concentrations, variable discharge, and subtle spatial gradients in stream chemistry is important for characterizing the vast number of poorly monitored headwater streams. PFMs have also only had limited applications in quantifying

hyporheic zone transport and could be tested further to uncover spatial variation in chemistry and discharge in these areas.

1.2.3. Solute fluxes in forested headwater catchments

Forested headwater catchments tend to export low dissolved loads that reflect mineral weathering, vegetation type, and atmospheric deposition rates (Herlihy et al. 1998, Clark et al. 2000, Watmough et al. 2005). The chemistry of forested headwater streams can change rapidly over relatively short stream lengths and time scales (Lawrence et al. 1990, Mulholland 1992, Wolock et al. 1997, Ensign et al. 2006). Thus, it is important when quantifying solute fluxes to use a sampling method that maximizes information gathered and still proves to be realistic for researchers and land managers.

Time-integrated, low cost sampling schemes, even in well-studied watersheds, are needed to characterize solute transport in areas that are difficult to monitor and to improve characterization in sub-catchments located within gauged catchments. The Hubbard Brook Experimental Forest (HBEF) in New Hampshire is a well-studied forested headwater catchment and a Long Term Ecological Research (LTER) site where stream chemistry has been studied for decades (Driscoll et al. 1989, Palmer et al. 2004, Likens 2017) and solute loads are very low (Likens et al. 2012). One major point of interest in forested headwater catchments including the HBEF is the transport and export of solutes, such as aluminum (Johnson et al. 1981), nitrogen (Ross et al. 2012), hydrogen ion (Driscoll et al. 1982), calcium (Likens et al. 1998), sulfur (Likens et al. 2002), and dissolved organic carbon (Gannon et al. 2015). Chemical variation in such solutes is evident at fine spatial and temporal scales at the HBEF, where headwater stream chemistry variability in a 41 ha sub-catchment is as significant as the variability in stream chemistry across the entire 2973 ha Hubbard Brook watershed (Zimmer et al. 2013). The focus on long-term export of solutes and

how that export may change over time provides insight on ecosystem change in response to disturbances, both natural and anthropogenic. However, these long term and resource intensive goals are met by the difficulty in capturing high temporal resolution information across large spatial scales. As such, HBEF is an example of a forested headwater catchment that could benefit from time-integrated solute flux analysis, as better characterization of spatial patterns in the context of documented long-term records can advance our understanding of the processes that drive chemistry changes in headwater streams.

1.2.4. Surface and subsurface solute transport

The chemistry of headwater streams at Hubbard Brook, like most headwater systems, is also affected by surface water-groundwater exchange, both along the stream and below the stream (Findlay 1995, Hall Jr et al. 2002). Therefore, watershed mass flux at any point along the stream network is the sum of the mass flux in surface water and subsurface water discharging at that location. The streams at Hubbard Brook are gauged at locations where bedrock outcrops at the surface, limiting any subsurface mass flux at those locations, which increases the confidence in watershed solute export estimates and mass balance calculations (Likens et al. 2006). However, in headwater sub-catchments above the watershed gauges, subsurface water, including near-stream seeps and springs, and lateral groundwater inputs from hillslopes, affects the chemical variability of streams in otherwise similar topographic environments. The contributions of seeps, springs and hillslope storage zones to streams vary depending on season and distance from the stream (Detty et al. 2010, Zimmer et al. 2013). PFMs can quantify solute fluxes in both the streams and the subsurface; thus, there is an opportunity to compare chemical changes along not only a longitudinal gradient in streams, but also as a vertical gradient between the surface and subsurface of streams (Hill et al. 1998, Kunz et al. 2017).

1.3. Research Objectives

The aim of this study is to evaluate how well PFMs characterize solute export from a forested catchment where the export is relatively well-known. HBEF was selected as the study site because of its continuous record of discharge, weekly water chemistry measurements, and long record of watershed mass balance, which can be used to validate the PFM approach. The results of this study will provide an improved approach for sampling watershed solute chemistry at locations throughout a stream network with limited or difficult access and estimating loads where discharge data are not collected. In addition, and perhaps more importantly, the proposed method has the potential to detect changes in water chemistry that may be missed with coarse sampling schemes such as from weekly, fixed point grab samples, and thus provide a more accurate representation of watershed export and variation in chemistry throughout stream networks.

This study has two main objectives:

1. Develop, implement, and evaluate a method using passive flux meters (PFMs) to characterize chemical water quality at the HBEF that is inexpensive and simple to replicate.
2. Use PFMs to examine the relative contribution of solute transport from the stream as represented by surface and subsurface water in tributaries at the HBEF.

I predict that mean concentrations estimated using PFMs will be the same as mean concentrations estimated by collecting periodic grab samples of stream and subsurface water and stream flow measurements. In addition, I predict that subsurface water sites will have higher mean concentrations and lower water fluxes through the PFM than surface water sites. The low

chemical concentrations in streams at the HBEF poses a new challenge for the PFM to quantify concentrations that are often at or near the limit of quantification of analytical instruments. In this context, the efficacy of the PFM to characterize water quality is tested in new environmental conditions.

2.0. Methods

2.1. Overview

This chapter describes the theory, construction, deployment, and retrieval of the passive flux meter (PFM) to characterize water flux and solute flux in three watersheds at the Hubbard Brook Experimental Forest (HBEF). It includes a site description of the HBEF and methods for calculating the cumulative discharge, cumulative solute fluxes, and mean solute concentrations using the PFM. These methods are detailed in subsequent sections, but an overview is provided below.

PFMs were constructed at the water quality laboratory at the HBEF. PFMs were deployed in streams at the HBEF to examine flow, solute load, and solute concentration in streams with contrasting chemistries representing dilute headwater stream systems. PFMs were composed of layers of granulated activated carbon (GAC) and ion exchange resin. The GAC was sorbed with a suite of pre-equilibrated alcohols that were used as tracers of water flux through the PFM. The mixed-bed anion-cation exchange resins were used to capture solutes at HBEF. PFMs were deployed in three watersheds at the HBEF over six different periods. PFMs were subsequently recovered and sampled for analysis. GAC samples were analyzed on a GC – FID for initial and final relative tracer mass. Cumulative discharge through each PFM was calculated using the proportional mass of each tracer remaining on the GAC after deployment. Resin samples were extracted using 2 x 2.0 M KCl extraction and analyzed on ICP – AES for total aluminum (Al), calcium (Ca), and sulfate as sulfur (S). These solutes were of interest in this study because they exhibit different spatial gradients in streams at HBEF (Likens et al. 2006). Ca is also an essential nutrient for plants and microbial organisms and has been historically depleted from soil exchange pools due acid deposition (Likens et al. 1998) which has included sulfate loading to HBEF as well.

Sulfate is still the dominant anion in stream water (Likens et al. 2002). Al has been a concern because it can be mobilized from forest soils in acidic conditions and has adverse impacts on soils, forest vegetation, and aquatic organisms (Palmer et al. 2002).

2.2. Passive flux meter theory and flux estimation

The PFM was designed similarly to PFMs that have been used in recent subsurface (Annable et al. 2005, Cho et al. 2007, Kunz et al. 2017) and surface water monitoring (Klammler et al. 2007, Padowski et al. 2009) applications, although the design was scaled down in size significantly for use in headwater streams. Previous studies using surface water PFMs utilized hydrodynamic designs to account for turbulent flows and for direct estimates of stream velocities (Klammler et al. 2007, Padowski et al. 2009). However, the designs were complex and not easily reproducible and the primary goal for this study was to characterize concentration and load and not stream velocity. For this study, a simpler design modified from groundwater PFM designs (Annable et al. 2005) was evaluated for use in streams. PFM design is shown in Figure 2.1. PFM construction is discussed in detail in section 2.3.

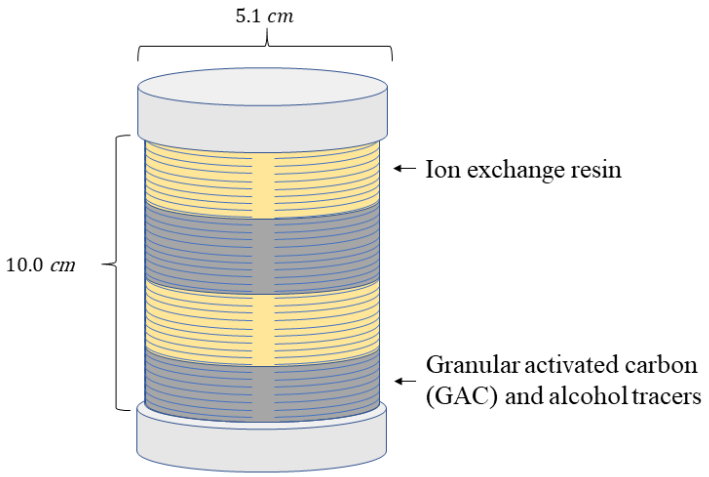

Figure 2.1. Passive flux meter design. The yellow shaded regions represent layers of ion exchange resin and the gray shaded regions represent layer of granular activated carbon (GAC).

2.2.1. Determination of water flux using alcohol tracers

Time-averaged horizontal water flux through the PFM is determined by loss of alcohol tracers, which are sorbed onto a GAC sorbent in the device. As water passes through the PFM, the tracers are eluted from the GAC at a rate that is proportional to the horizontal water flux, q_x, through the device. The change in relative mass of tracer over the deployment period is used to determine q_x. The ability for each tracer to elute from the GAC is a function of its initial relative mass and retardation factor, R_D. R_D is the ratio of the velocity of water through the PFM to the velocity of the tracer through the PFM. Values of R_D above 1.0 indicate that the tracer velocity through the PFM is lower than the water velocity. Multiple tracers with different R_D values allow multiple estimations of water flux through the PFM as well as an increased probability that there will be at least one tracer present on the GAC after deployment in flowing water.

Time-averaged horizontal water flux through the PFM, also referred to as the Darcy flux, $q_x\ \left[\frac{m}{s}\right]$, is a function of the radius of the sampler, $r\ [m]$, the porosity of the GAC sorbent, $\theta\ [-]$, the relative tracer mass remaining on the sorbent after deployment, $\mathrm{M}_R\ [-]$, the retardation factor of the tracer, $R_D\ [-]$, and the deployment time, $t\ [s]$ (Hatfield et al. 2004, Annable et al. 2005, Cho et al. 2007):

$$q_x = \frac{1.67 r \theta (1-\mathrm{M}_R) R_D}{t} \tag{2.1}$$

This equation is valid only when tracer elution from the GAC is linear; this occurs when the relative mass of tracer remaining (M_R) in the PFM sorbent is greater than 30% for the tracers used in this study (Hatfield et al. 2004). After recovery of a field-deployed PFM, the tracers are extracted from the GAC with isobutanol (IBOH), so they can exist in solution and be quantified using analytical instrumentation. The relative tracer mass remaining on the sorbent after

deployment, M_R $[-]$, is determined using the initial mass of tracer per mass GAC, M_i $\left[\frac{m}{m}\right]$, and final masses of tracer per mass GAC, M_f $\left[\frac{m}{m}\right]$, in solution.

$$M_R = \frac{M_f}{M_i} \tag{2.2}$$

M_i is calculated using the concentration of tracer in each GAC sample, C_i $\left[\frac{mg}{L}\right]$, the volume of IBOH extractant in each sample vial, V_{iso} $[L]$, and the mass of GAC $[mg]$ in each sample, m_{GAC}. M_f is calculated similarly.

$$M_i = \frac{C_i * V_{iso}}{m_{GAC}} \tag{2.3}$$

$$M_f = \frac{C_f * V_{iso}}{m_{GAC}} \tag{2.4}$$

Water flux estimations by the PFMs in this study were based on retardation factors and elution rates of alcohols measured by Annable et al. (2005). The GAC used here was the same manufacturer and product type used in previous PFM studies (Hatfield et al. 2004, Annable et al. 2005, Cho et al. 2007, Kunz et al. 2017). Thus, following Kunz et al. (2017), the same partitioning characteristics and retardation factors for each alcohol tracer that have been previously quantified were used in this study, eliminating the need for in-line GC sampling to produce alcohol elution dynamics. The linear relationships between pore volumes of water through the PFM and tracer elution was shown by a column elution test performed by Annable et al. (2005). The data from the column elution test show that for methanol and ethanol, the curves are linear until about 30% of the initial tracer remains on the GAC and isopropyl and tert-butyl alcohol are linear over much larger ranges of pore volume (Figure 2.2). The retardation factor, R_D $[-]$, for each tracer is determined using:

$$R_D = 1 + \frac{K_D \rho_B}{\theta} \tag{2.5}$$

where the partitioning coefficient between the sorbed phase and the aqueous phase of each tracer is K_D $\left[\frac{mL}{g}\right]$, the porosity of the GAC sorbent is θ $[-]$, and the bulk density of the GAC sorbent is ρ_B $\left[\frac{g}{mL}\right]$. Retardation factors for the alcohol tracers were taken from Annable et al. (2005) and are provided in Table 2.1.

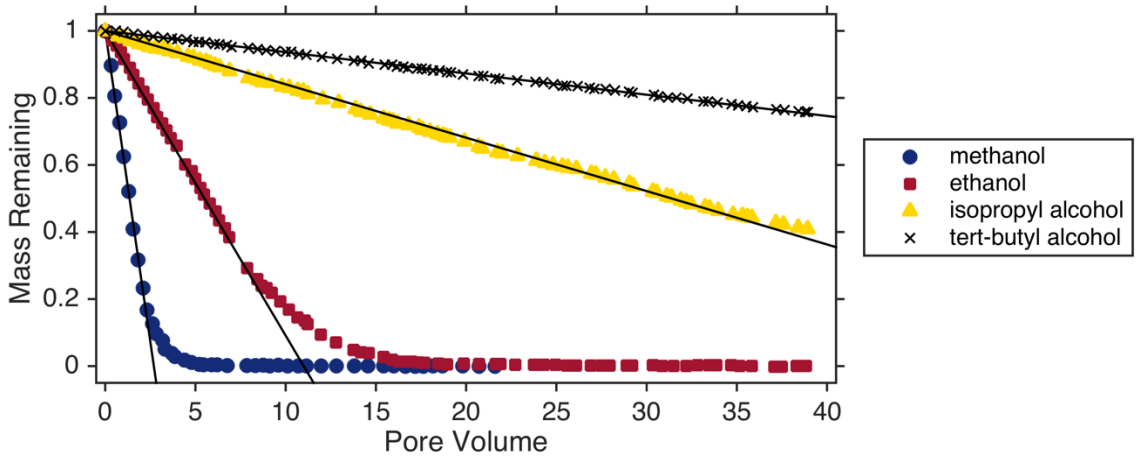

Figure 2.2. Elution of alcohols from granular activated carbon (GAC) as a function of pore volumes from a flow-through column (Annable et al. 2005). Each of the four tracers, methanol (MeOH), ethanol (EtOH), isopropyl alcohol (IPA), and tert-butyl alcohol (tBA) have unique elution rates from GAC. R_d (Table 2.1) was taken from Annable et al. (2005) and was determined from the straight-line portion of the alcohol elution data.

Table 2.1. Initial concentrations and retardation factors of tracers in equilibration solution used in Annable et al. (2005) and assumed for this study (modified from Annable et al. 2005).

Resident tracers	Aqueous concentration (g L^{-1})	R_d
Methanol (MeOH)	1.2	4.9
Ethanol (EtOH)	1.2	20
Isopropyl alcohol (IPA)	2.3	109
tert-Butyl alcohol (tBA)	2.3	309
2,4-Dimethyl-3-pentanol (DMP)	1.2	> 1000

In addition to water flux through the PFM, the cumulative discharge through the PFM can also be calculated using the column elution curves from Annable et al. (2005). Assuming the same elution dynamics for each tracer in the laboratory column and the field-deployed PFM, the cumulative pore volumes of water that pass through the column, $\xi\ [-]$, can be calculated using the relative mass of tracer remaining on the sampler, M_R. ξ represents the x-axis of Figure 2.2 and the linear portion of the curves allows for the calculation of pore volumes. Therefore, using the cumulative pore volumes through the sampler, the porosity of the GAC, θ, and the volume of the tracer layer, V_{PM}, the cumulative discharge through the PFM is calculated using the following equation:

$$Cumulative\ Discharge\ Volume\ (L) = \xi * \theta * V_{PM} \tag{2.6}$$

2.2.2. Determination of flow-weighted concentration using ion exchange resin

PFMs were loaded with an ion exchange resin sorbent to capture solutes of interest (Al, Ca, and S) during a deployment period. A mixed-bed of cation (sulfonic acid) and anion (quaternary ammonium) exchange resin can capture both anions and cations in the water column simultaneously (Yang et al. 1991, Langlois et al. 2003). The cations and anions sorbed onto the ion exchange resins were extracted using a KCl solution. I evaluated various methods of extracting the ion exchange resins, which are discussed in section 2.3.2. The total mass of solute extracted from the resins was used to determine the flow-weighted mean concentration of solutes:

$$Mean\ Concentration\ \left(\frac{mg}{L}\right) = \frac{solute\ mass\ extracted\ (mg)}{PFM\ cumulative\ discharge\ volume\ (L)} \tag{2.7}$$

2.3. Passive flux meter construction

2.3.1. Composition of GAC layer and tracer solution preparation

Each PFM contained two layers of GAC which provided two separate estimates of discharge through the sampler that were averaged. The GAC was a 12 x 40 mesh X-262 silver impregnated activated carbon manufactured by Bestech, Inc. Before PFMs were constructed, a tracer solution was prepared to mix with the GAC. The tracers used in this study were methanol (MeOH), ethanol (EtOH), isopropyl alcohol (IPA), tert-butyl alcohol (tBA), and 2,4-dimethyl-3-pentanol (DMP). Product information for the alcohol tracers is provided in Table 2.2. DMP was used as an internal standard due to its very high R_D; thus, it should not elute over the PFM deployment period of days to a couple of weeks at typical environmental flow rates. To ensure that DMP loss did not invalidate PFM data, values of M_R for the four other tracers were normalized to loss of DMP for each PFM deployment.

Table 2.2. Product information for alcohols used in this study.

Tracer	MeOH	EtOH	IPA	tBA	DMP	IBOH
CAS – No.	67-56-1	64-17-5	67-63-0	75-65-0	600-36-2	78-83-1
Weight %	>95	99 - 100	>95	>95	94	≥ 99.5
Specific Gravity at 20 °C	0.791	0.785	0.785	0.780	0.820	0.802

A stock solution was prepared by mixing 100 mL MeOH, 100 mL EtOH, 200 mL IPA, 200 mL tBA, and 66 mL DMP. After combining thoroughly, the tracer solution was prepared by mixing a ratio of 13 mL stock solution to 1.0 L of deionized water to 1.5 L of dry GAC. The tracer solution

was prepared in a Teflon-sealed HDPE container, shaken thoroughly, and refrigerated at 4 °C while not in use.

2.3.2. Composition of resin layer and ion exchange resin pre-treatment

The ion exchange resins used in this study were a mixed bed of Amberlite IRA 400 (Cl^- form) anion exchange resins and Amberlite IR 120 (H^+ form) cation exchange resins. It was important for any background contamination present on the ion exchange resins to be removed for the resins to effectively characterize cations and anions at the field site. Therefore, the resins were pre-treated with extracting solution before deployment into water systems (Langlois et al. 2003, Fenn et al. 2004). Extraction methods for ion exchange resins vary, but typically involve either a drip-through exposure to an extracting solution (Yang et al. 1991) or an equilibration-style extraction of multiple exposures to an extracting solution (Kolberg et al. 1997, Kjonaas 1999). In most resin studies, 2.0 M KCl has been used as the extractant as it has been shown to be effective in displacing ions from the resin exchange sites and avoiding degradation of the resin bead structure (Kolberg et al. 1997, Kjonaas 1999, Susfalk et al. 2002).

In this study, Amberlite IRA 400 (Cl^-) and Amberlite IR 120 (H^+) were mixed at a 1:1 equivalency ratio to provide an opportunity for equal sorption of cations and anions. Table 2.3 provides information from the resin manufacturers regarding density, ion exchange capacities, and subsequent mixture ratios. For each 100 g of dry resin mixture, 63.0 g of IRA 400 and 37.0 g of IR 120 were combined in a nylon filter bag. The resins were pretreated at a ratio of 3:1 (mL extractant : g resin) using an extracting solution of 2.0 M HCl in a flow-through system similar to the system used by Yang et al. (1991). The filter bag was rinsed thoroughly with deionized water before being placed in a plastic funnel placed on a stand to collect acid waste. Three additions of 100 mL 2.0 M HCl were added in succession to the funnel, allowing the acid to drip through the

filter bag to pre-treat the resins. After adding 300 mL of HCl, the resin filter bag was thoroughly rinsed again with deionized water and resins were stored saturated in deionized water at 4 °C until construction of the PFM. Resins were pre-treated as close as possible to the time of PFM construction to ensure that resins remained saturated during PFM construction.

Table 2.3. Product information for ion exchange resins.

Resin	Amberlite IRA 400 (Cl^- form)	Amberlite IR 120 (H+ form)
Description	Anion Exchange Resin	Cation Exchange Resin
Total Exchange Capacity	1.40 meq / mL	1.80 meq / mL
Moisture Holding Capacity	40 – 47%	53 – 58%
Bulk Density	0.72 g / mL	0.80 g / mL

2.3.3. Assembling PFMs

PFMs were prepared using screened schedule 40 PVC with a diameter of 5.08 cm (2-inch nominal pipe) and a screen size of 0.25 mm spaced every 6.7 mm. The PVC was cut into 10 cm segments, and two PVC caps were used as ends for each segment. PFMs were rinsed thoroughly with deionized water and dried before construction. Monofilament mesh filter bags with a pore size of 300 μm were used to house the sorbent materials, and rubber washers with an outer diameter of 5.08 cm were used to separate sorbent layers. Each PFM also contained a 1.27 cm diameter CPVC tube inserted through the center of the screened PVC to hold the rubber washers in place and provide structure to the filter bag. Before the first layer was packed, a clean rubber washer was

placed through the CPVC tube, the tube was placed in the filter bag, and the filter bag was placed in the PVC housing. The bottom layer was packed first, and layers were packed in alternating order of resin and GAC sorbent. The first layer was packed with 30 g of wet pre-treated resin. Specific care was taken not to compress the sorbent layers. A rubber washer was placed on the CPVC tube to create the base for the next layer. The second layer was packed with 25 g of wet GAC equilibrated with alcohol tracers. This process was repeated for the upper two layers of sorbent. Initial samples were taken for each PFM constructed to calculate the initial mass of tracers relative to mass of GAC. While the PFM was being packed, 10.0 g of wet GAC was transferred to a 40 mL borosilicate glass vial with Teflon septa containing 30 mL of IBOH. These samples were tightly shut and refrigerated at 4 °C until analysis.

When the PFM was packed with its four layers, the top of the filter bag was tied tightly shut using Teflon tape. The PFM was capped and refrigerated at 4 °C until deployment. Figure 2.3 displays the layers of the PFM and the closure of the filter bag. Masses of each sorbent layer were recorded to calculate bulk density. The value of 0.55 was used for porosity, θ, of the GAC sorbent, as this is the same product used in previous PFM studies (Hatfield et al. 2004, Annable et al. 2005, Cho et al. 2007).

PFMs were constructed the day of installation for each deployment and refrigerated at 4°C until installation phase to minimize tracer losses through volatilization before exposure to the stream.

Figure 2.3. Photographs of PFM assembly showing layers and filter bags. In the left photograph, PFMs were built in layers of alternating GAC (black) and resin (brown). Once packed, they were tied shut with Teflon tape (right) before being capped.

2.4. Study Area, PFM deployment and recovery

2.4.1. Study area

The Hubbard Brook Experimental Forest (HBEF) is a 2,973-ha research forest in the southern White Mountains of New Hampshire. The climate is humid continental with short, cool summers and long, cold winters. The mean temperature is -8.3 °C in January and 18.7 °C in July (Likens 2013). Roughly one-third of the annual precipitation of 1400 mm falls as snow, and about one-half of the annual runoff occurs during the spring snowmelt period (Bailey et al. 2003). The soils are generally characterized as well-drained Spodosols of sandy loam texture (Likens 2013);

however, recent work has described the soils as variants of podzols with a broad range of drainage classes, soil morphology, and soil development history (Bailey et al. 2014, Gillin et al. 2015). The bedrock at the HBEF is composed of pelitic schist and calc-silicate granulite from the Silurian Rangeley Formation, overlain by sandy loam glacial till left by the retreat of the late Wisconsinian glacier about 14,000 years ago (Likens 2013, Bailey et al. 2014). Weathering of bedrock due to deep seepage is uncommon at the HBEF due to the compaction of the glacial till (Lawrence et al. 1990, Likens 2013). The dominant vegetation at Hubbard Brook is northern hardwoods, consisting of sugar maple (*Acer saccharum*), yellow birch (*Betula alleghaniensis*), and American beech (*Fagus grandifolia*). At higher elevations, such as the ridgetops surrounding the valley, balsam fir (*Abies balsamea*), red spruce (*Picea rubens*), and mountain white birch (*Betula cordifolia*) are more dominant (Likens 2013). The Hubbard Brook Valley is a key study area for observing and quantifying the processes that control headwater stream chemistry because it is relatively undisturbed by anthropogenic influence, as it has not been logged extensively since 1920, apart from tree removal in specific experimental watersheds (Lawrence et al. 1986).

Three watersheds at the HBEF were used in this study: Watershed 3 (W3), Watershed 9 (W9), and Zig Zag Brook watershed (ZZ). PFMs were deployed at the outlet of each of these three watersheds. Figure 2.4 displays the HBEF and each of the study watersheds. W3 is a reference catchment with a south-facing aspect and exhibits a distinct chemical gradient from top to bottom of the watershed (Zimmer et al. 2013). At the top of the watershed a pH of between 4.00 – 4.50 has been observed while circumneutral pH has been observed at the watershed outlet. W9 is a north-facing watershed that displays low pH and high concentrations of Al and DOC throughout its stream reach (Palmer et al. 2005). ZZ is a north-facing watershed in the southwestern portion of the valley that does not have a weir or a long history of chemical measurements; however, grab

samples of stream water chemistry have been observed to have higher relative Ca compared to most streams in the Hubbard Brook Experimental Forest and circumneutral pH from top to bottom of the watershed (Likens et al. 2006). Figure 2.5 displays the spatial pH from Likens et al. (2006). These three watersheds exhibit the same range of variability of chemistry observed in the entire Hubbard Brook Valley, and thus, were adequate watersheds in which to test the efficacy of the PFM. In addition, the presence of weirs at both W3 and W9 allows for high temporal resolution measurements of discharge to validate the water flux estimate with the PFM. The discharge at ZZ is not known continuously and thus ZZ served as a surrogate watershed to test the efficacy of the PFM to estimate mean concentration of solutes over a deployment period where weekly grab samples are not collected and instantaneous discharge is not measured.

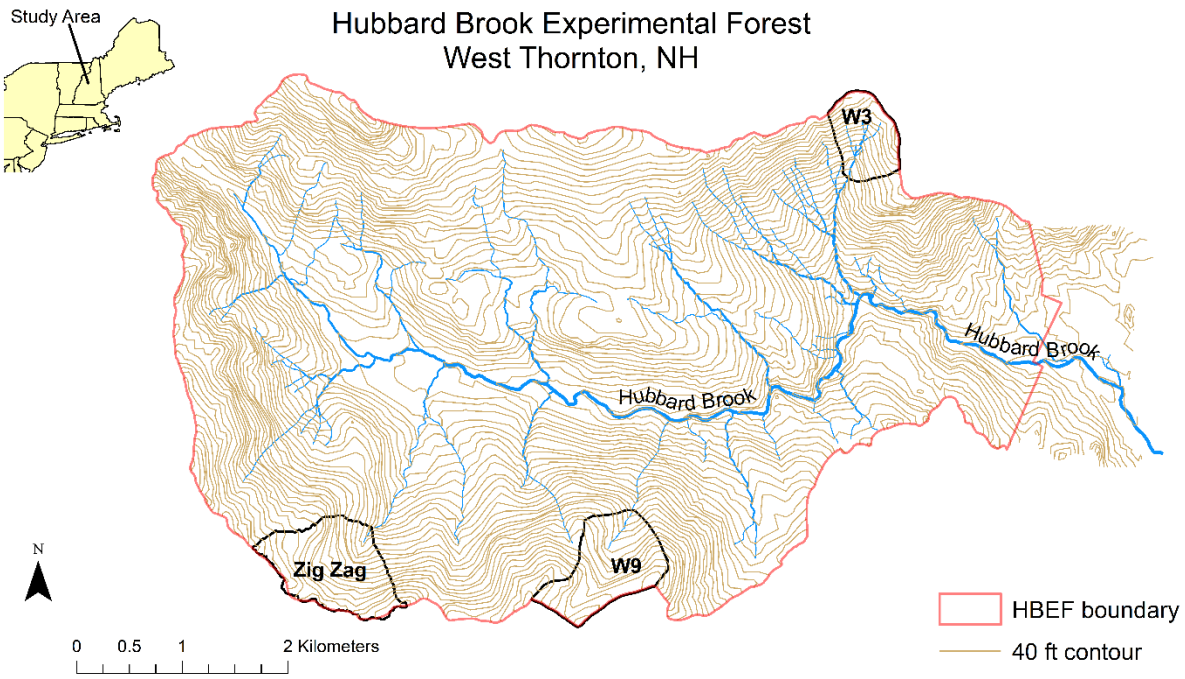

Figure 2.4. Map of the Hubbard Brook Experimental Forest, West Thornton, NH. Watershed 3 (W3) is a gauged reference catchment that has been sampled since 1963. Watershed 9 (W9) is a gauged reference catchment that has been sampled since 1995. Zig Zag Brook is an ungauged north-facing stream.

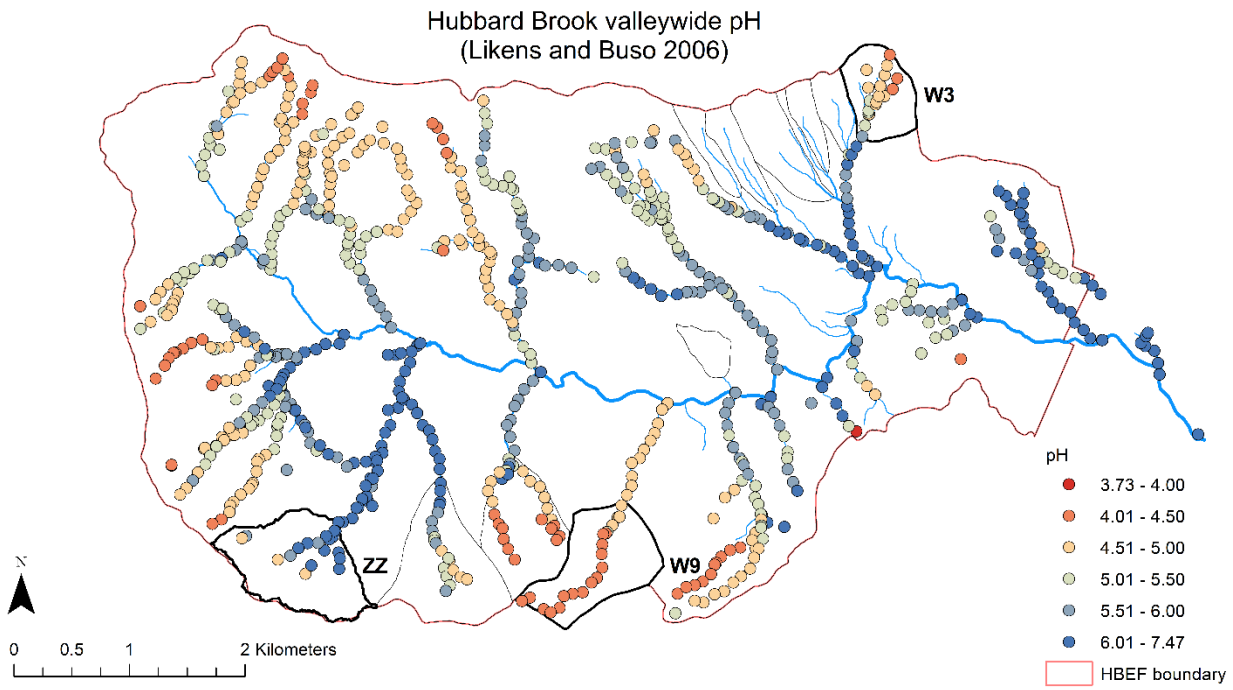

Figure 2.5. The pH of headwater streams at the Hubbard Brook Experimental Forest. Data were collected as part of a valley-wide sampling study (Likens et al. 2006).

To further examine the spatial variation in chemistry within W3 and to examine the relative contributions of surface and subsurface water to stream export, two tributaries were selected as additional study sites to test the efficacy of the PFM in solute concentration estimation. Tributary W-3 and tributary E-4 (Figure 2.6) were selected as additional sites due to the contrast in chemistry along the stream reach before they join Paradise Brook, the main stream within W3. In these tributaries, three sites were selected to examine longitudinal differences in chemistry: an upstream site, an intermediate site, and a downstream site. Tributary W-3 displays relatively higher pH and Ca than tributary E-4 throughout the year (Zimmer et al. 2013).

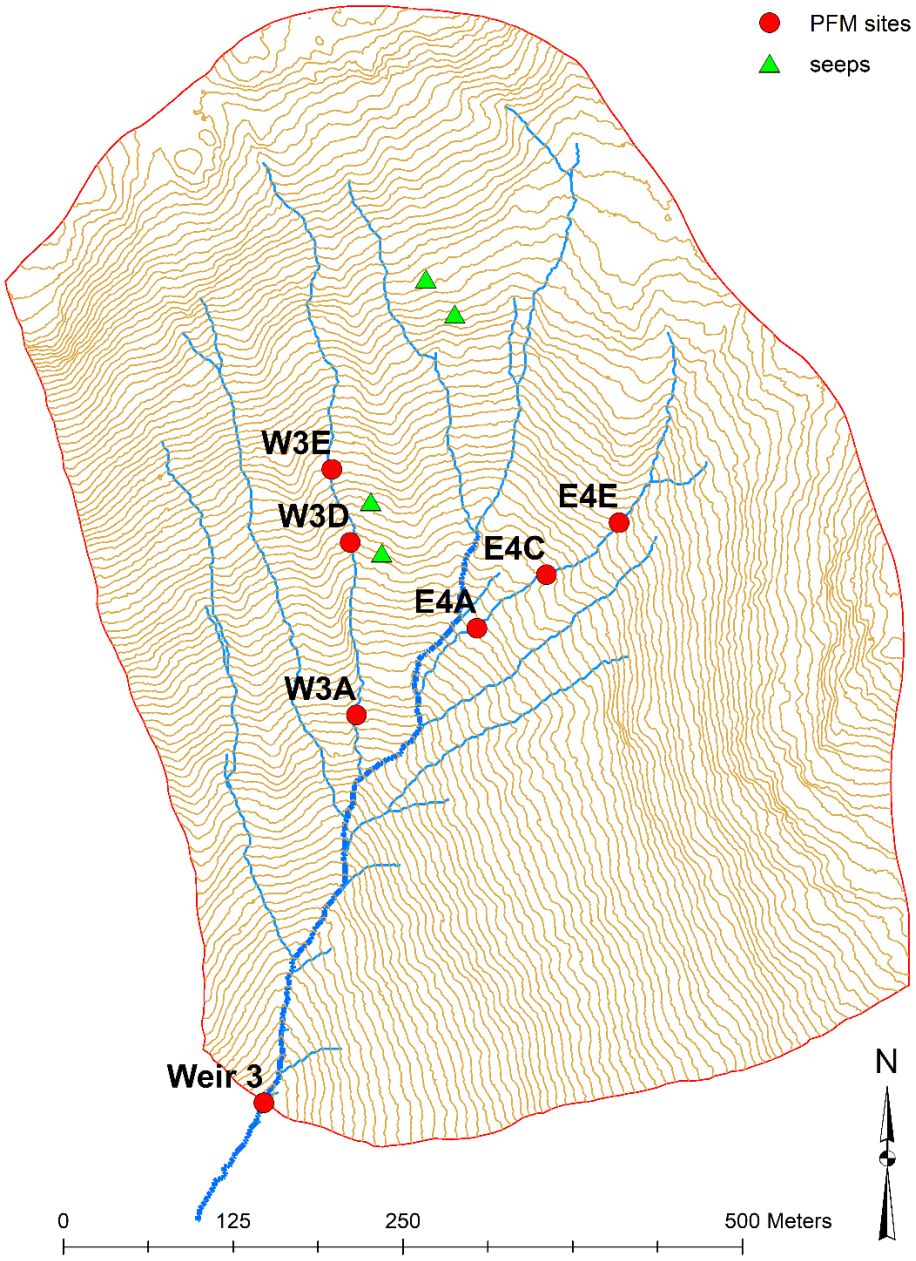

Figure 2.6. Tributary sites within Watershed 3 (W3) for surface / subsurface PFM deployment. Green triangles represent seeps that discharge perennially to the stream. Red circles represent the PFM deployment sites, including the outlet PFM at the weir of W3. Streams have been displayed with a combination of 0.5 ha upslope area flow accumulation and data from field validation stream surveys.

2.4.2. PFM deployment

Deployment time is important to consider in PFM monitoring studies, as there needs to be sufficient mass of tracer remaining on the GAC to quantify tracer concentrations. In addition, there needs to be enough solute mass on the resin to quantify extractable solutes above the detection limit, but the solute mass collected on the resin cannot exceed the sorption capacity of the mixed-bed resins. In this context, there is an optimal deployment time that balances these two constraints. The deployment time for each PFM was chosen at 7 days due to a potential for low proportion of interception of flow by the PFM design and due to the low chemical concentrations in streams at the Hubbard Brook Experimental Forest. In general, this is a longer deployment time than previous PFM surface water studies (Klammler et al. 2007, Padowski et al. 2009).

PFMs were used in six deployment periods at the HBEF (Table 2.4). The first five were week-long deployments at the outlets of W3, W9, and ZZ. Four of these deployments took place during the summer of 2017, and the last deployment occurred during November of 2017, when flow was significantly higher in all three watersheds compared to the summer deployments. The sixth deployment of PFMs took place in November in two tributaries within W3 (tributary W-3 and tributary E-4) to examine the longitudinal variation in chemistry along these streams. For each tributary, three sites were chosen for PFMs (Figure 2.6). PFMs were installed in both the surface water and the subsurface 10 cm below the stream bed.

Brass anchors were drilled into the bedrock at each site to secure to PFMs in place for the surface water installations. Angle steel bars were attached to the anchors using hose clamps, and PFMs were attached to the angle steel bars using hose clamps. For the subsurface sites, 5.08 cm diameter wells were installed 10 cm below the surface. These wells had the same screen length as the PFMs. To deploy the subsurface PFMs, PFMs were placed on top of the well and gently pushed

down to the bottom of the well using a steel rod. Figure 2.7 displays the layout of the surface and subsurface PFMs at each site.

Two control PFMs were constructed for each PFM deployment. The purpose of the control PFMs was to assess the potential for tracer loss during transport from lab to field site and during deployment of PFMs into stream sites. Both controls were constructed using the exact method as for the other PFMs. The first control PFM, referred hereafter as a deployment control, was constructed and brought to the ZZ site during each installation of the PFM. It was deployed into the stream, immediately retrieved, and sampled on the same day it was constructed. The second control PFM, referred hereafter as a transport control, was constructed, brought to the ZZ site during installation, brought immediately back to the lab and sampled on the same day it was constructed.

Table 2.4. PFM deployment schedule.

Deployment Date	Deployment Sites*	Water Sample Collection Dates
7/18 – 7/25	ZZ, W3, W9, TC, DC	7/17, 7/24
7/25 – 8/01	ZZ, W3, W9, TC, DC	7/31
8/01 – 8/08	ZZ, W3, W9	8/01, 8/5 (13 samples), 8/6, 8/7, 8/8
8/09 – 8/16	ZZ, W3, W9, TC, DC	8/09, 8/14
11/07 – 11/14	ZZ, W3, W9, TC, DC	11/7, 11/8, 11/9, 11/10, 11/11, 11/12, 11/13, 11/14
11/09 – 11/15	Tributary W-3, Tributary E-4	11/09, 11/15

* ZZ is Zig Zag, W3 is watershed 3, W9 is watershed 9, and W-3 and E-4 are two tributaries in watershed 3. DC and TC are deployment and transport controls, respectively.

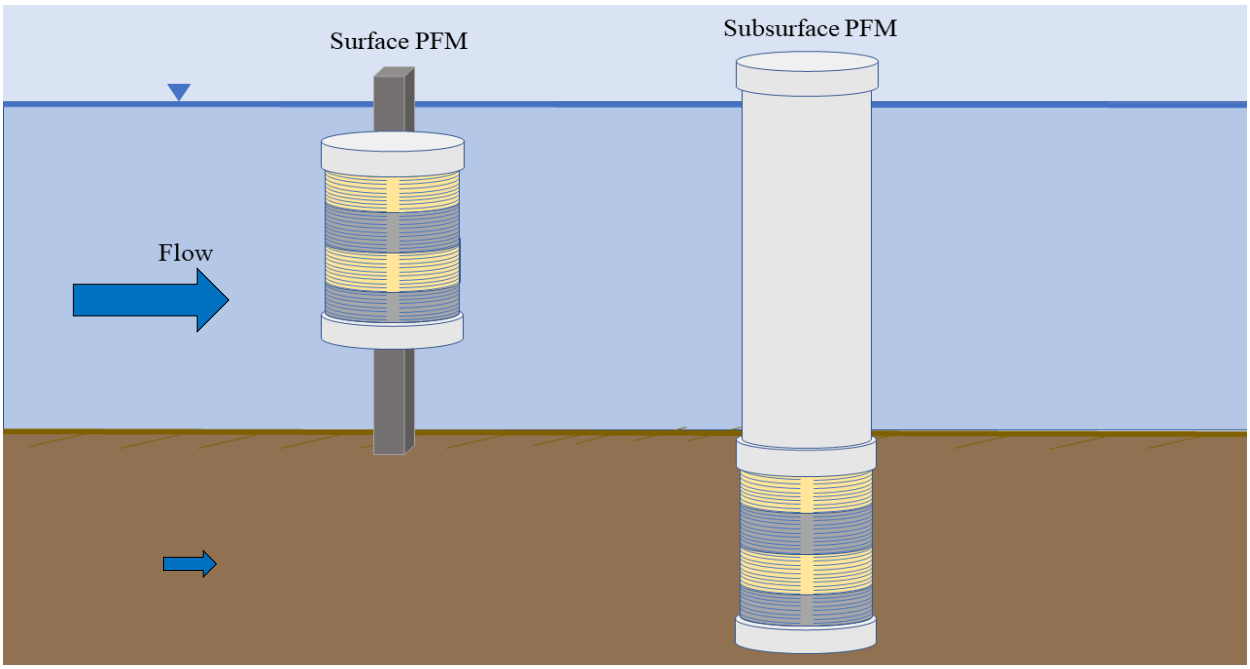

Figure 2.7. Schematic of PFM deployment in the surface and subsurface water in tributaries W-3 and E-4. Surface and subsurface PFMs were placed within 2 m of each other at all sites. Gray regions of the screen represent layers of GAC, and yellow regions represent layers of ion exchange resins.

2.4.3. Water sample collection during PFM deployment and mean stream velocity estimation

During each PFM deployment, water samples were collected to compare to estimations made by the PFM. Table 2.4 displays the water samples collected during each deployment. Water samples were filtered with 0.45 μm glass fiber filters and frozen before being analyzed via Inductively Coupled Plasma – Atomic Emission Spectroscopy (ICP – AES) at the US Forest Service Water Quality Laboratory in Durham, NH using HBEF water quality protocols. Samples were analyzed for concentrations of aluminum (Al), calcium (Ca), and total sulfur (S). Method detection limits for aluminum, calcium, and sulfur were 0.014 mg L^{-1}, 0.040 mg L^{-1}, and 0.110 mg L^{-1}, respectively. Limits of quantification (LOQ), or the values above which analytical variability is within 10% of the measured value, were 0.075 mg L^{-1} for Al, 0.25 mg L^{-1} for Ca, and 0.50 mg L^{-1} for S. Average concentrations in stream water were determined using the integration method, the protocol currently used by the HBEF (Buso et al. 2000). Using this method, I reported the grab sample concentrations for days on which grab samples were collected and reported the average concentration of grab samples for days between samples.

2.4.4. PFM recovery and sampling

At the end of each deployment, PFMs were recovered from deployment locations, taken back to the laboratory at the HBEF, and deconstructed for analysis. Each layer was removed individually, homogenized, subsampled, and refrigerated at 4 °C until laboratory analysis. Each resin sample was transferred into 30 mL plastic scintillation vials, and each final GAC sample was transferred into 40 mL borosilicate glass vials with Teflon septa containing 30 mL of IBOH extractant. Each PFM contained 5 samples: 2 resin samples, 1 initial GAC sample, and 2 final GAC samples. All samples were sent to Virginia Tech and stored at 4 °C until extracted and analyzed.

2.5. Laboratory analysis and calculations

2.5.1. Analysis of GAC for tracer concentrations

Each initial and final sample of GAC was shaken on a shaker table on LOW for 24 hours prior to subsampling into GC vials. After shaking, samples settled for 24 hours before decanting the liquid into 2 mL GC vials. Each sample was analyzed on an Agilent 6850 Series II Gas Chromatograph with Flame Ionization Detector (GC – FID) at Virginia Tech. The GC-FID used a Restek MXT 624 Capillary Column (30 m length, 0.53 mm ID, 3 μm film thickness) to quantify concentrations of MeOH, EtOH, IPA, tBA, and DMP in each initial and final sample of GAC. The method for GC-FID analysis is discussed in Appendix A.

M_R for each PFM layer was calculated using equation (2.3) and (2.4). Cumulative discharge for each PFM was calculated using the data from Figure 2.2 and equation (2.5). Mean cumulative discharge was calculated by averaging the mean discharge estimated from each tracer within both layers of the PFM. Recovery of each tracer using GC – FID was calculated using prepared standards run as unknowns during sample analysis. Tracer recovery was within $\pm 2\%$ for each of the five tracers.

2.5.2. Ion exchange resin extraction and analysis via ICP – AES

Each resin sample was extracted using a 2 x 2.0 M KCl extraction protocol first described by Kjonaas (1999). A test was conducted in the laboratory before extracting resin samples to calculate the extraction efficiency of this method. Resin subsamples were extracted with five extractions of 1.0 M KCl and 2.0 M KCl to compare the extraction methods. Extraction efficiency for two extractions was calculated by dividing the extracted mass from two extractions by the

extracted mass from five extractions. Mean extraction efficiency for 1.0 M KCl was 85.5% for calcium and 98.1% for sulfur, while mean extraction efficiency for 2.0 M KCl was 91.6% for calcium and 100% for sulfur (Figures 2.8 and 2.9).

After validating the 2 x 2.0 M extraction method, 5.0 g of resin from each sample was transferred to a 250 mL bottle and filled with 60 mL of 2.0 M KCl, providing a 1:12 ratio of resin mass to extractant volume. Samples were shaken on a shaker table on LOW for 1 hr. Once shaken, extractant solution was collected by pouring the solution through pre-washed Nitex filter paper to prevent the resins from being collected in the solution. After the first extraction sample was collected, 60 mL of 2.0 M KCl was again added to the sample bottle, samples were shaken again for 1 hr., and the second extraction was collected using Nitex filter paper. All extract samples were diluted to 1.0 M KCl and run via ICP-AES at the Virginia Tech Soil Testing Lab in Blacksburg, VA. For 1.0 M KCl samples, method detection limits on the ICP-AES for aluminum, calcium, and sulfur were 0.006 mg L^{-1}, 0.026 mg L^{-1}, and 0.025 mg L^{-1}, respectively. The limit of quantification (LOQ) was 0.50 mg L^{-1} for all three solutes. Total mass of solutes extracted from resins was calculated by multiplying the concentration from the ICP-AES by the sample volume and scaling by the proportion of exchange resin in the sample to the total mass resin in the PFM. Mean concentration estimated by the PFMs were then calculated using equation (2.7).

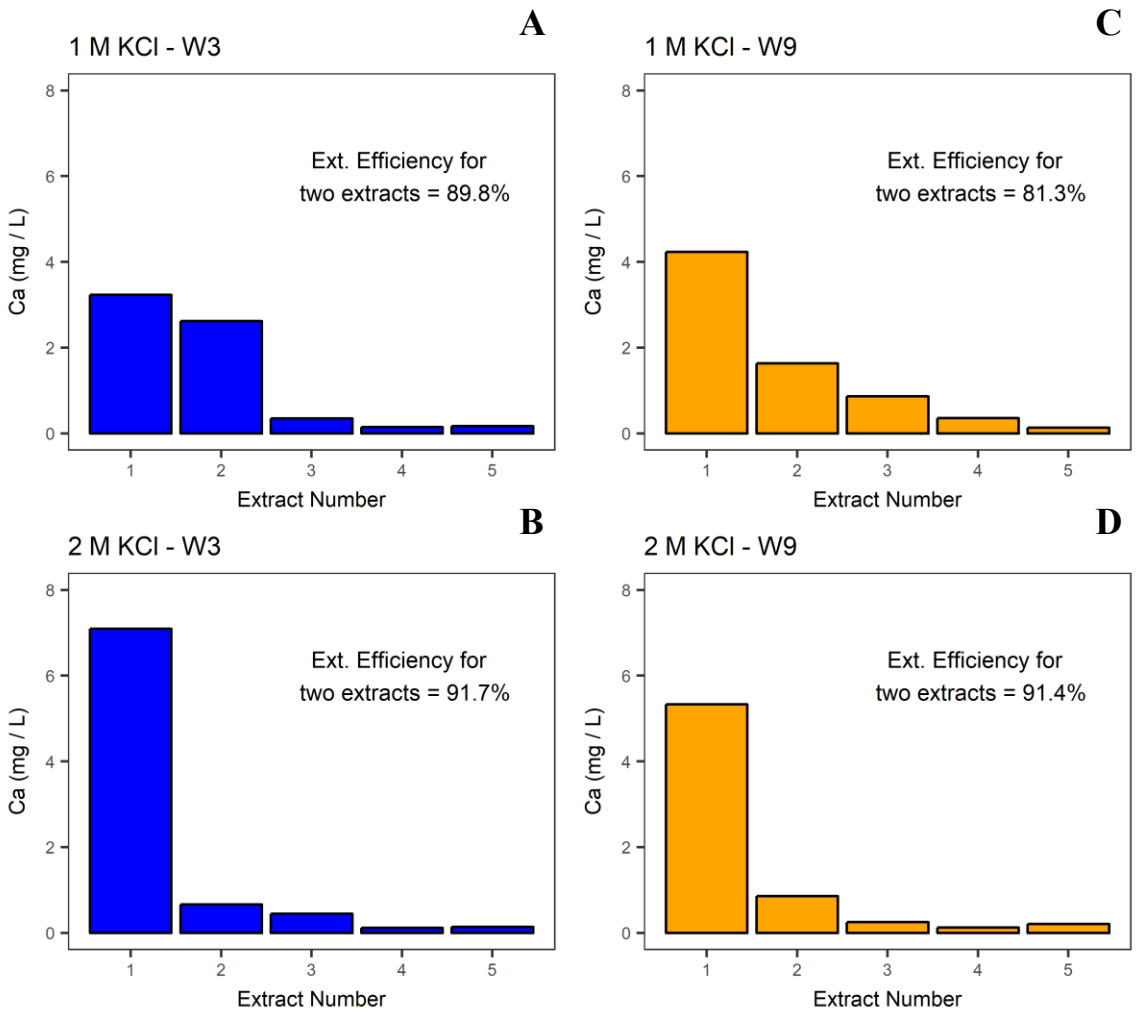

Figure 2.8. Resin extraction test for calcium. The 2 x 2.0 M KCl extraction method was tested against other proposed methods for extracting calcium from ion exchange resins. Subsamples of a W3 PFM were extracted with 1.0 M KCl (**A**) and 2.0 M KCl (**B**). This was repeated for subsamples of a W9 PFM (**C, D**). Extraction efficiency were calculated by dividing the total mass extracted from the first two extractions by the total mass extracted for five extractions.

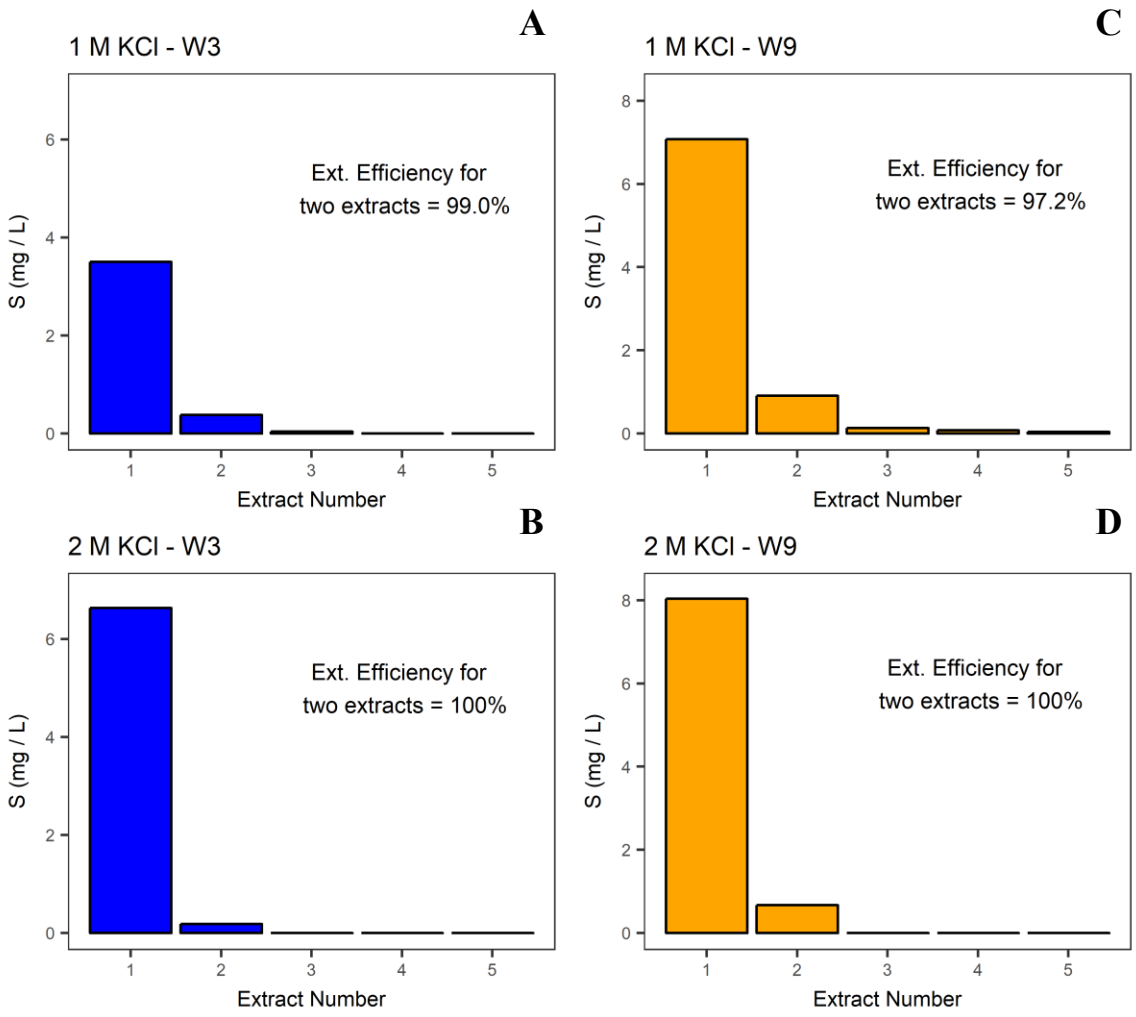

Figure 2.9. Resin extraction test for sulfur. The 2 x 2.0 M KCl extraction method was tested against other proposed methods for extracting calcium from ion exchange resins. Subsamples of a W3 PFM were extracted with 1.0 M KCl (**A**) and 2.0 M KCl (**B**). This was repeated for subsamples of a W9 PFM (**C, D**). Extraction efficiency were calculated by dividing the total mass extracted from the first two extractions by the total mass extracted for five extractions.

3.0. Results

3.1. PFM deployment conditions

During the five outlet PFM deployments, stream discharge and chemistry was different between W3 and W9 (Figure 3.1). Three of these five deployments occurred at baseflow, and two were high flow conditions. A storm occurred during third PFM deployment (8/01 – 8/08), but the discharge response was only significant at W9 with an almost two orders of magnitude increase in flow while W3 only increased by 5 times. The fifth deployment (Figure 3.1 B & D) occurred during the falling limb of a rain event in the fall when stream discharge was much larger in W3 and discharge in W9 was comparable to the storm event during the third deployment. For the three baseflow deployments (7/18 - 7/25, 7/25 – 8/01, 8/09 – 8/16), concentrations of calcium at W3 ranged from 0.7 to 0.9 mg L^{-1}, while during the high-flow deployments (8/01 – 8/08, 11/07 – 11/14), concentrations of calcium at W3 ranged from 0.6 to 1.1 mg L^{-1}. Similar dynamics occurred at W9 and for sulfur concentrations (0.8 to 1.2 mg L^{-1}) showing that the variation in stream concentrations was low.

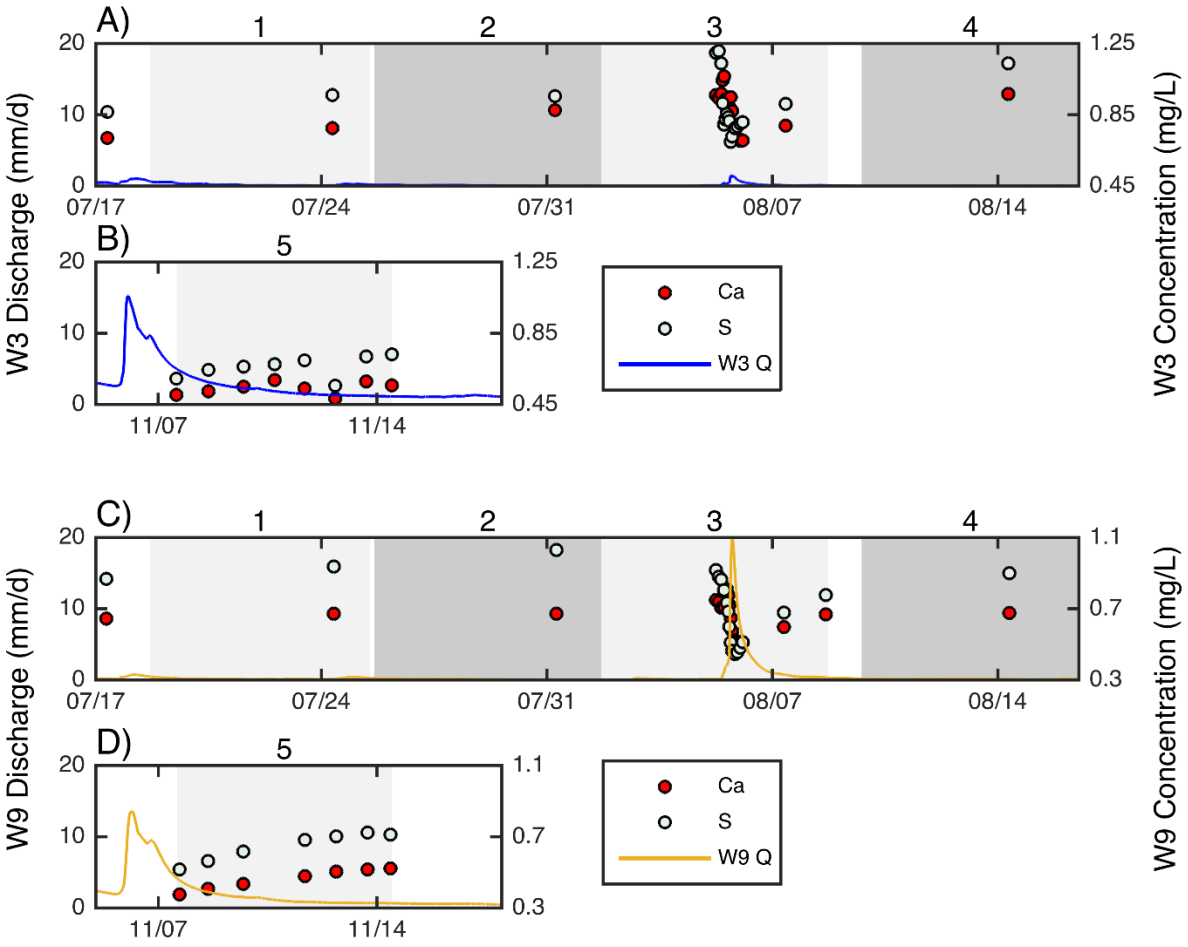

Figure 3.1. PFM deployment weir discharge (mm day^{-1}) and grab sample chemistry (mg L^{-1}) for W3 (**A (**summer**), B (**fall**)**) and W9 (**C (**summer**), D (**fall**)**). Numbers at the top of each plot (1-5) denote the deployment number and correspond with the gray shaded regions of the time series. Grab samples were collected during each deployment to determine mean deployment concentrations. Concentrations of calcium are shown in red, and concentrations of sulfur are shown in light green.

3.1. Cumulative discharge through PFMs

Cumulative discharge was calculated for each PFM deployment. The cumulative discharge through the PFM and Darcy flux through the PFM were highly correlated ($R^2 = 0.997$) (Appendix B). The ratio of these different representations of flow through the PFM provide an estimate of the effective cross-sectional area of flow through the PFM cylinder, which was 11.1 cm^2 and given by the inverse of the slope of the figure in Appendix B.

In general, cumulative discharge through the PFM was highest in Zig Zag Brook (ZZ) and lowest in Watershed 9 (Figure 3.2). The exception to this trend occurred during the 8/01 deployment, where weir discharge at W9 increased by almost two orders of magnitude over a two-day period. During this storm event deployment, W3 and ZZ PFMs did not experience appreciable stormflow. The measured channel velocity at W9 increased from less than 0.5 cm/s to over 30 cm/s for several hours, while measured channel velocity at W3 increased from 2 cm/s to over 14 cm/s for the same duration.

Subsurface PFM water fluxes were higher than surface water fluxes in the sixth PFM deployment (Figure 3.3). For some subsurface sites, particularly the tributary E-4 sites, only tBA, the tracer with the largest retardation factor, was present on the GAC after deployment.

At least two tracers were present within the valid range of M_R for every PFM deployed at all three watershed outlets, so discharge estimates were calculated using the mean of at least two tracers. During the first deployment period, appreciable mass of DMP was lost (~35%). The high R_D of this alcohol indicates that it should not have eluted. For all other deployments, DMP was recovered with a mean M_R of 1.01 ($\pm$0.03, n = 61). This means that, on average, 100.01% of DMP was recovered at the end of the deployment period over the sample range. Values of M_R for each tracer were normalized to loss of DMP. I found four instances where the discharge estimates were

not significantly different from the transport control PFM estimates using Tukey's Honest significant difference pairwise hypothesis tests (alpha = 0.05). These PFMs were W9 (7/18), W9 (7/25), W3 (7/25), and W9 (8/09). These PFMs were removed from concentration estimations. Mean cumulative discharge for the deployment controls were 0.15 L ($\pm$ 0.13 L, n = 8). Mean cumulative discharge for the transport controls were 0.07 L ($\pm$ 0.08 L, n = 8). Control PFMs were not built for the deployment 8/01 – 8/08.

The estimation of discharge through the PFMs varied with each tracer. Excluding controls from analysis, estimation of PFM discharge using the tBA tracer was closest to the mean estimate using all tracers remaining on the PFM, with a deviation of 18% from the mean estimate of discharge (Figure 3.4). The mean discharge estimates for all tracers were normalized to 1.00 and are shown by the dashed line in Figure 3.4. I found that the lower weight tracers (e.g. MeOH and EtOH) consistently underpredicted the mean discharge through the PFM if used alone. IPA also underpredicted the mean discharge through the PFM. However, tBA estimation of discharge was primarily above the mean estimate of discharge for all tracers.

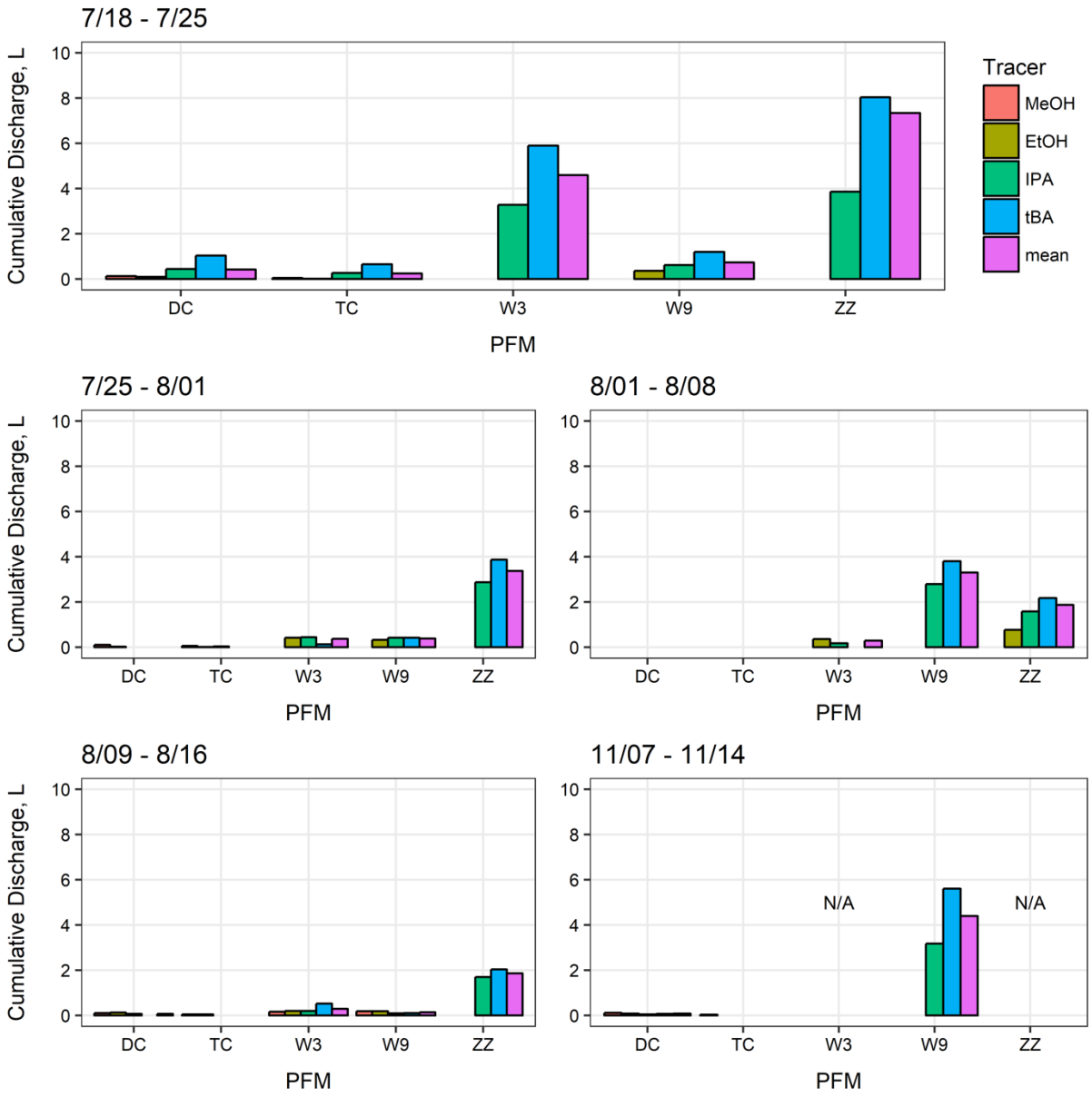

Figure 3.2. Cumulative discharge through the PFM for outlet deployments, in L. Discharge was calculated for the deployment control (DC), transport control (TC), Watershed 3 weir (W3), Watershed 9 weir (W9), and the Zig Zag Brook outlet (ZZ). Discharge was calculated separately for each tracer remaining on the GAC within the range $0.30 < M_R < 1.00$. Values of N/A are given for PFM deployments where no alcohol tracer was recovered with a value of M_R within the appropriate range.

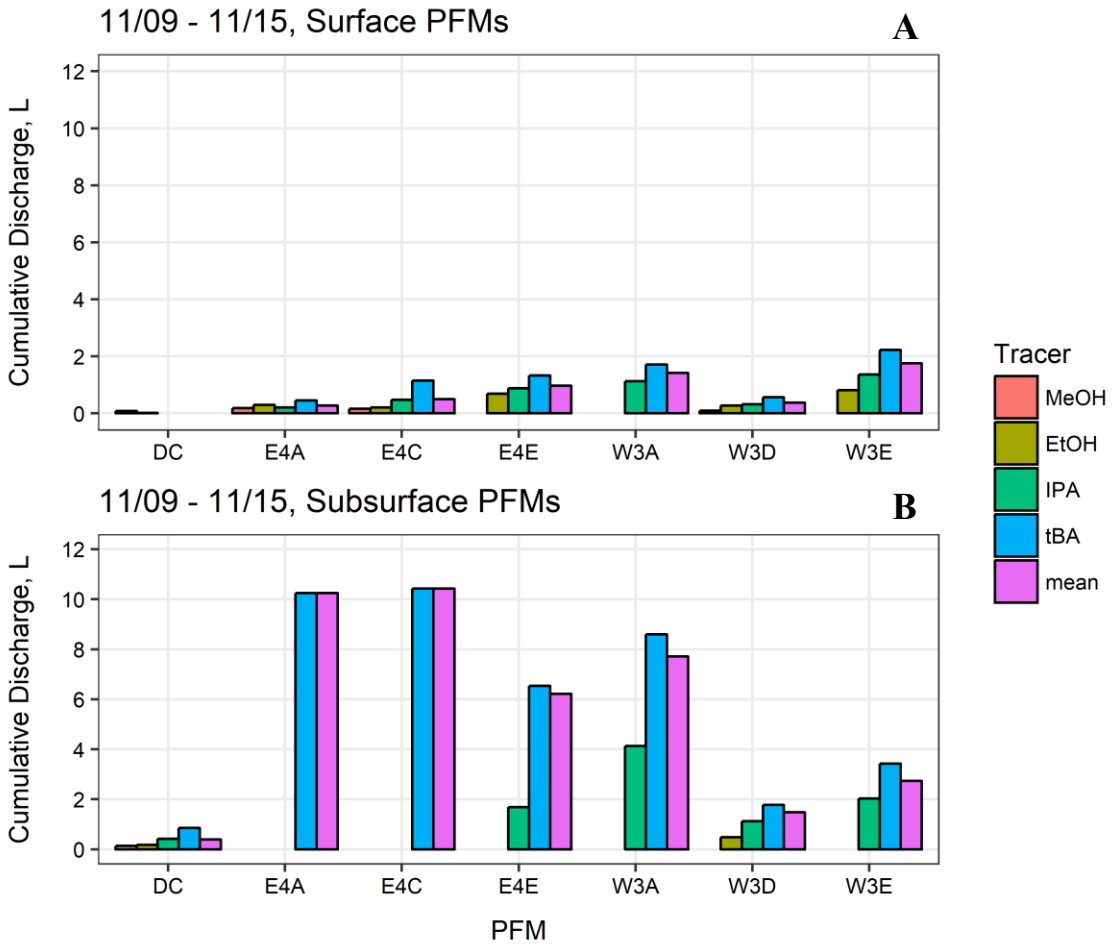

Figure 3.3. Cumulative discharge through the PFM for surface (**A**) and subsurface (**B**) deployment, in L. Discharge was calculated for the deployment control (DC), transport control (TC), tributary E-4 sites listed downstream to upstream (E4A, E4C, E4E), and tributary W-3 sites listed downstream to upstream (W3A, W3D, W3E). Discharge was calculated separately for each tracer remaining on the GAC that was in the range $0.30 < M_R < 1.00$.

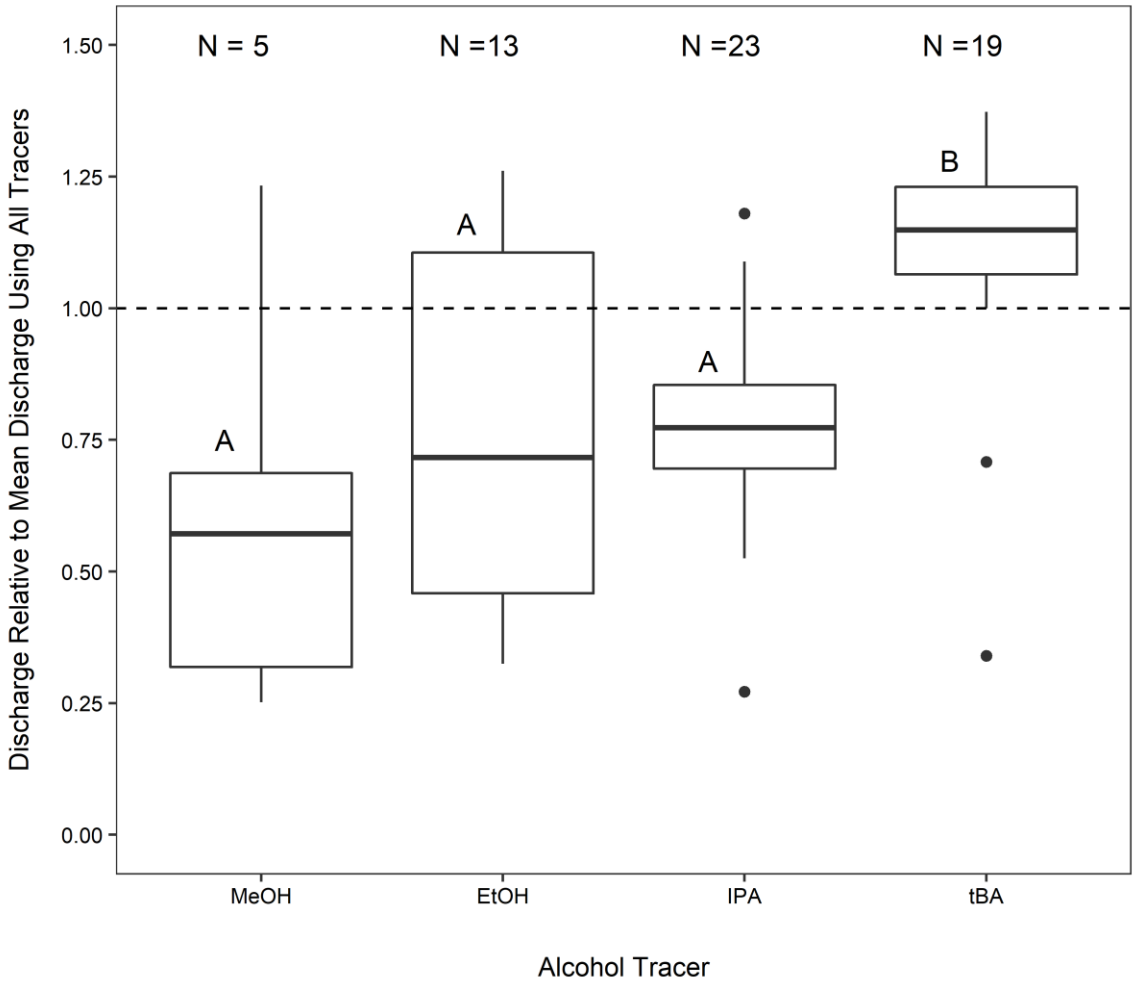

Figure 3.4. Variability in discharge estimates through the PFM by tracer used with control PFMs removed from analysis. Mean values of discharge are normalized to 1.00 and shown by the dashed line. Results from Tukey's Honest Significant Difference pairwise hypothesis tests are provided with letters. MeOH, EtOH, and IPA were not significantly different in their estimates of cumulative discharge, while tBA was significantly different from the other tracers.

3.2. Mean concentrations estimated using PFMs

Concentration relationships between resins and grab samples were examined for aluminum, calcium, and sulfur. Aluminum concentrations measured by the resins and grab samples were below the LOQ for over 75% of samples and therefore aluminum was removed of the concentration comparisons. Flow-weighted average concentrations of calcium and sulfur estimated by the PFM tended to be higher than grab sample estimates. Coefficients of determination were low for calcium and sulfur. R^2 for sulfur was 0.27 ($p = 0.001$), while the coefficient of determination for calcium was not significant. For calcium, 5 PFMs were within 10% of grab sample concentrations and 7 PFMs were within 30% of grab sample concentrations. For sulfur, 4 PFMs were within 10% of grab sample concentrations and 7 PFMs were within 30% of grab sample concentrations (Figure 3.5). When the cumulative discharge volume through the PFM was 1 L or above, estimated concentrations from the PFM were closest to grab sample concentrations. PFMs overestimated concentrations compared to grab samples in baseflow conditions.

PFMs deployed at the outlet of Watershed 3 were especially variable (Figure 3.6). The resin calcium concentrations at W3 ranged from 0.8 to 8.3 mg L^{-1}, while the resin sulfur concentrations at W3 ranged from 0.3 to 5.3 mg L^{-1}. However, grab sample concentrations at W3 ranged from 0.7 to 0.9 mg L^{-1} for calcium and 0.9 to 1.1 mg L^{-1} for sulfur. For the outlet PFMs, the majority of resin concentration estimations were near the estimations of calcium and sulfur made using grab samples; however, correlations were weak. R^2 for sulfur was 0.26 ($p = 0.029$), while the correlation for calcium was insignificant.

The PFMs that were deployed in the tributaries had resin concentrations of calcium and sulfur that were higher in surface PFMs than in subsurface PFMs (Figure 3.7). The subsurface

PFMs that were closest to grab sample concentrations had more cumulative discharge through the device; however, water flux through the subsurface was likely much lower than in the surface water. The concentrations estimated by the PFMs were more variable than grab sample concentrations in both the surface water and the subsurface water of tributary E-4 and tributary W-3 (Figure 3.7).

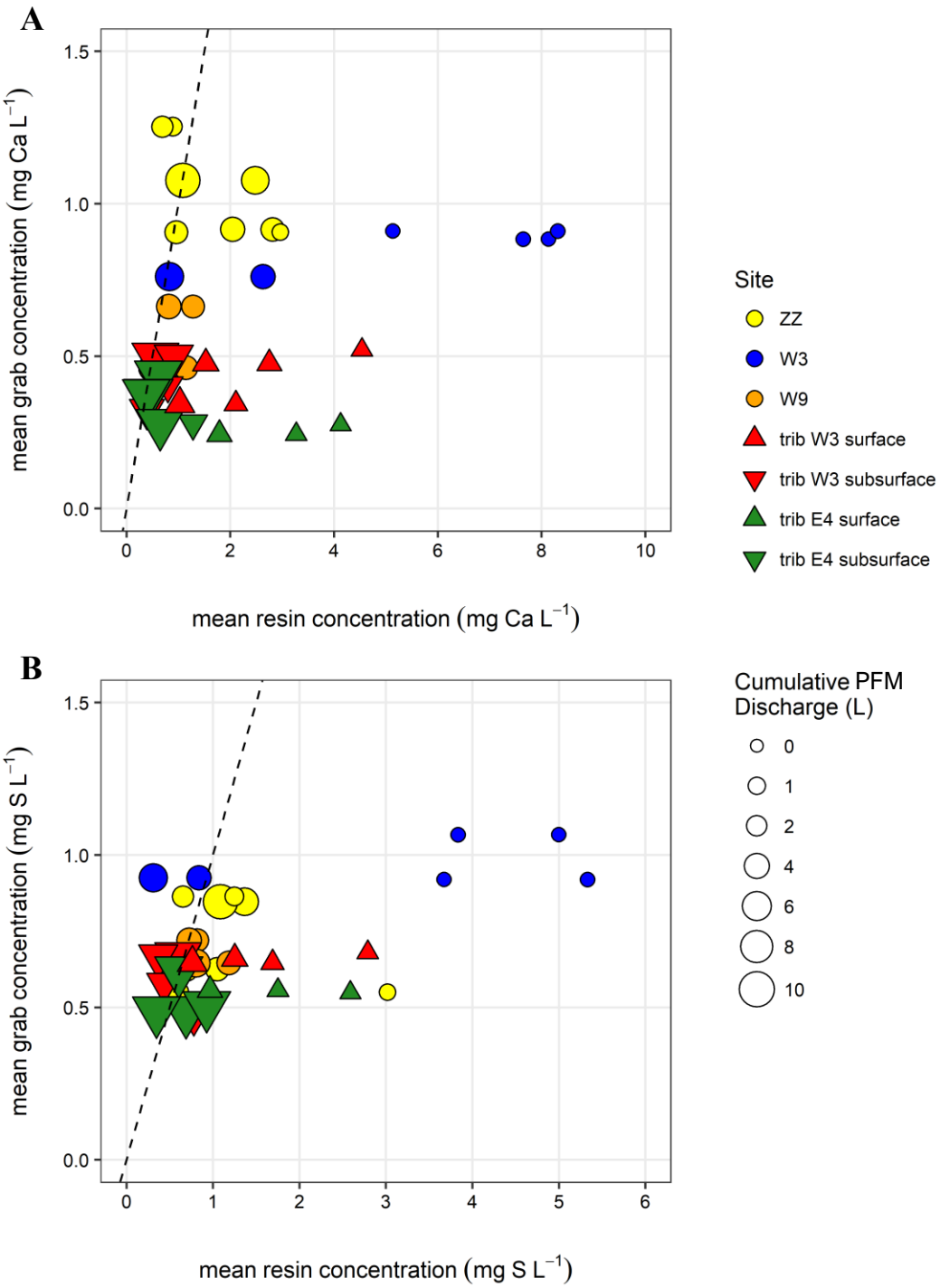

Figure 3.5. Resin concentration vs. grab sample concentration of calcium (**A**) and sulfur (**B**) for all PFMs. Mean resin concentration was calculated by dividing the total solute load on the resin by the cumulative discharge through the PFM. Dashed line represents a 1:1 relationship between resin concentration and grab sample concentration. Linear regression was not significant for calcium comparison. R^2 for sulfur comparison was 0.27 ($p = 0.001$).

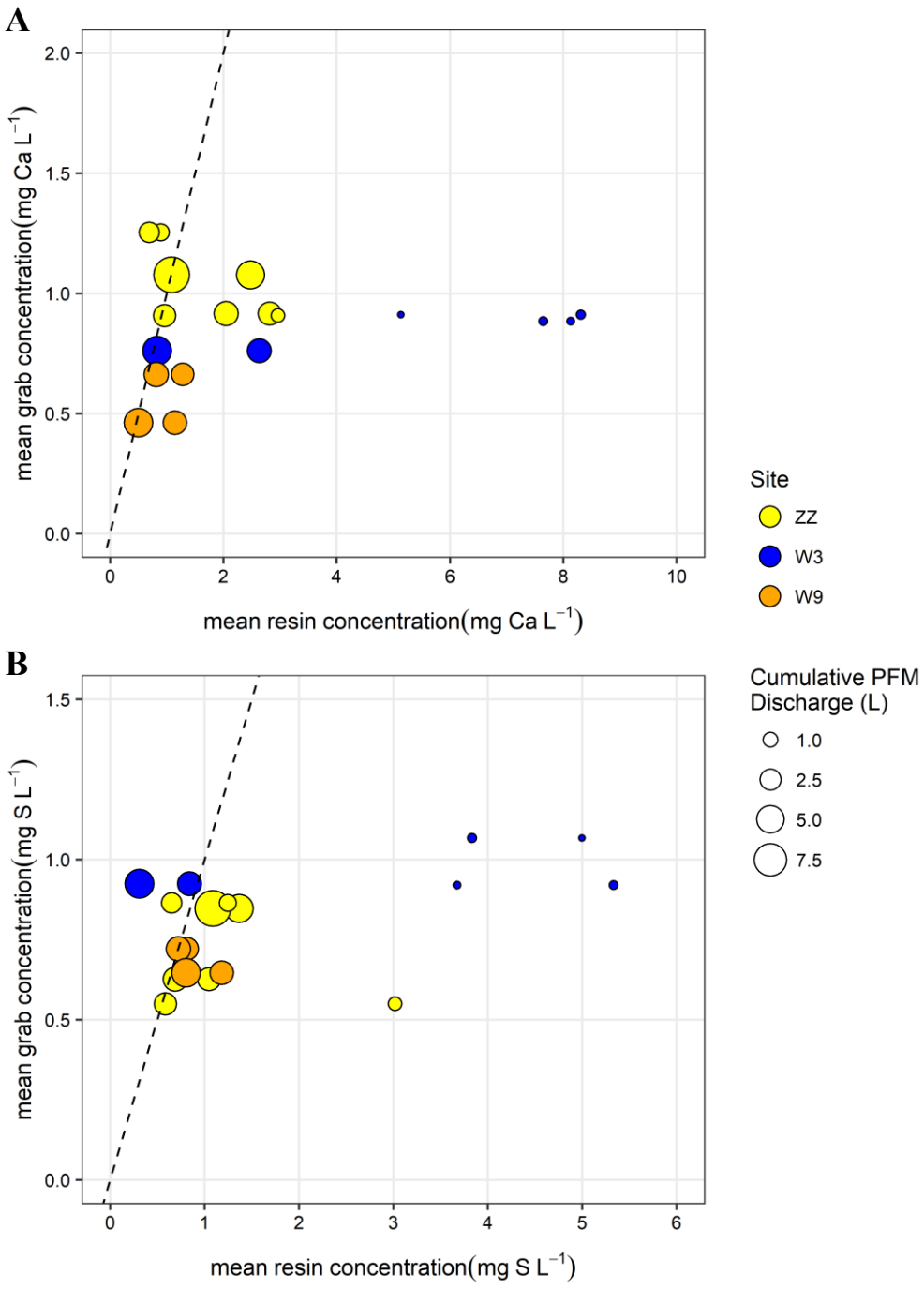

Figure 3.6. Resin concentration vs. grab sample concentration of calcium (**A**) and sulfur (**B**) for outlet PFMs. Point size is scaled by cumulative discharge through the PFM. Mean resin concentration was calculated by dividing the total solute load on the resin by the cumulative discharge through the PFM. Dashed line represents a 1:1 relationship between resin concentration and grab sample concentration. Linear regression was not significant for calcium comparison. R^2 for sulfur comparison was 0.26 ($p = 0.029$).

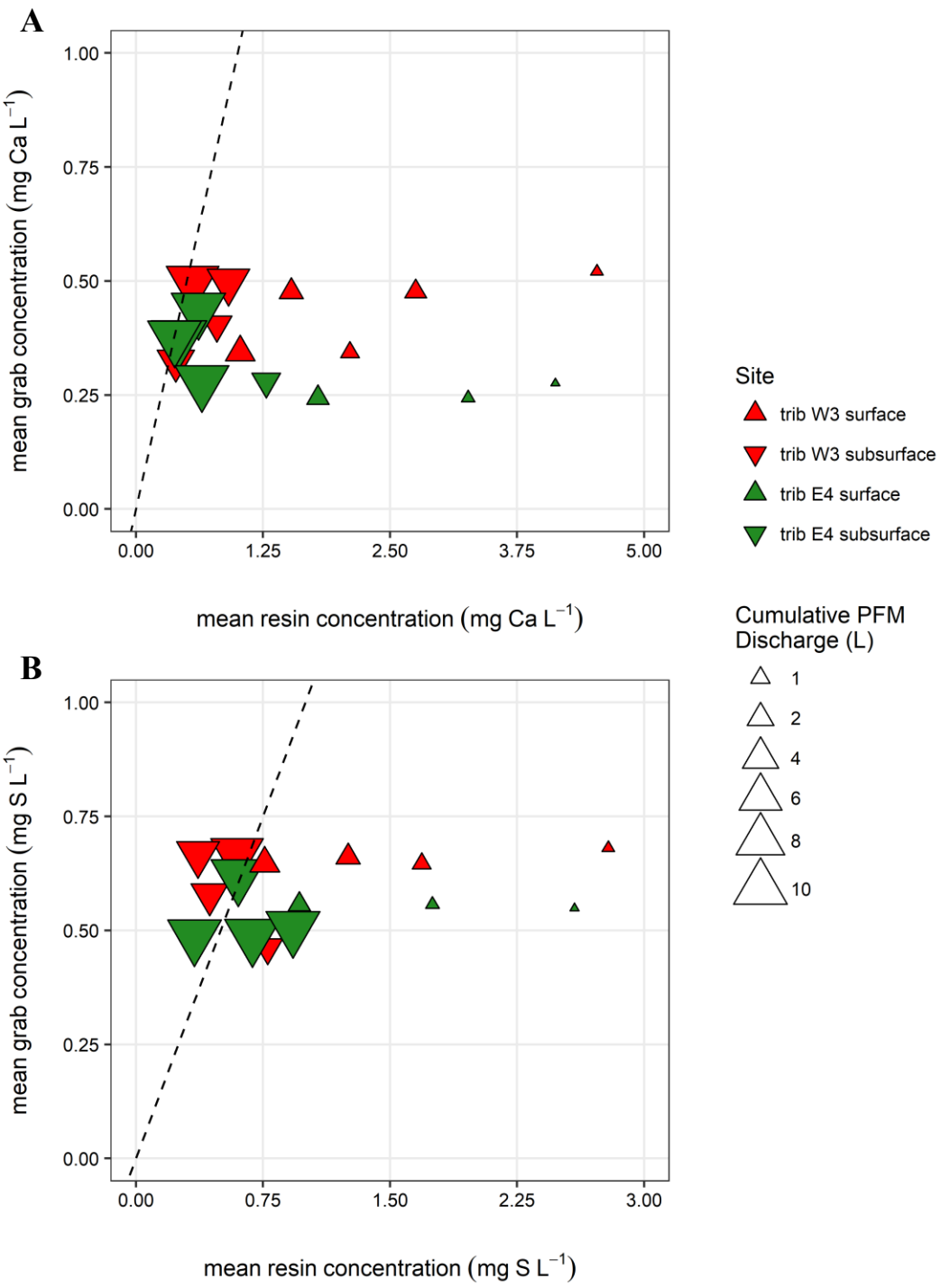

Figure 3.7. Resin concentration vs. grab sample concentration of calcium (**A**) and sulfur (**B**) for headwater PFMs. Resin concentration was calculated by dividing the total solute load on the resin by the cumulative discharge through the PFM. Dashed line represents a 1:1 relationship between resin concentration and grab sample concentration. Linear regression was not significant for calcium or sulfur comparison.

4.0. Discussion

4.1. Application of passive flux meters in a dilute headwater catchment

The application of the passive flux meter (PFM) was assessed under variable flow conditions and dilute stream water at the HBEF. The objectives of the study were addressed by designing, implementing, and deploying PFMs during baseflow and storms to address chemical variability in forested headwater streams. Flow-weighted average concentrations estimated by the PFMs were closest to grab sample concentrations at higher flows and overestimated grab sample concentrations at baseflow conditions, with the overestimation becoming more severe at extremely low flows in summer deployments.

The use of PFMs to characterize surface and subsurface solute concentrations was also addressed in this study. I hypothesized that subsurface water sites would have high mean estimated concentrations and lower cumulative discharge than surface water sites. However, I found that the surface water sites had higher concentrations and lower cumulative discharge through the PFM than their subsurface counterparts. There are several potential reasons for the inconsistent performance of the PFM in this study, which are discussed below.

4.2. Variability in estimating mass load and discharge using PFMs

There are several ways that PFM estimates of concentration may differ from grab sample estimates of concentration. First, laboratory methods have some inherent error derived from methodological choice, instrumentation error, and human error. PFMs estimates of concentration involve two independent quantities: 1) solute mass load and 2) discharge through the PFM. Depending on the resin extraction procedure used and the ability to remove all sorbed constituents from the resins, the solute mass load quantified in solution from the resins contains potential error. Furthermore, the resins may have inherent inefficiencies of sorption depending

on manufacturer, pre-treatment type, and handling procedures before, during, and after PFM installation. All of these conditions will affect the solute load estimates from the PFM.

4.3. PFM Performance under different flow conditions

While previous studies have shown PFMs can accurately estimate ambient stream velocity (Klammler et al. 2007, Padowski et al. 2009), few have tested the PFMs in streams with variable discharge over longer deployment times with dynamic velocities during the evaluation period. This poses a challenge in using the PFM, due to the changing pressure and velocity head in a stream channel over dynamic discharge conditions. At low flow velocities, simple cylindrical PFM designs are appealing to ensure an appreciable head difference across the device; however, at higher stream velocities this design has the potential to affect the flow around the device (Klammler et al. 2007). The larger cumulative discharge that was observed occurring through the subsurface water PFMs compared to the surface water PFMs may be due to streamflow diverging around the sampler at high stream velocities. The cylindrical design of the PFM with its vertical orientation in the stream and narrow slot width on the screen create potential divergent flow around the sampler.

4.4. Interception of flow around a cylinder

The effect of streamflow conditions on flowlines around a vertically oriented cylinder depends on the Reynolds number of the stream, Re (i.e.,vL/ν where ν is stream velocity, L is a characteristic length and is typically related to the hydraulic radius of the channel, and ν is the kinematic viscosity) and the drag coefficient of the device, C_D (Tritton 2012). As these streams have cascades and high velocities, flow is likely turbulent with high values for Re. For stream velocities that occur most often at the HBEF (between 0.05 and 0.5 m s^{-1}) and hydraulic radii near

0.05 m, Re is likely above 2000. At these Reynolds numbers, the drag coefficient of a cylinder in the water is near 1.0 (Tritton 2012). Using this drag coefficient, the relationship between stream conditions and divergence (and alternatively, interception) of flow around a permeable cylinder can be approximated (Bhattacharyya et al. 2006, Yu et al. 2011, Pinar et al. 2015). The Darcy number, Da, of the permeable cylinder, which represents the relative effect of the permeability of the GAC and resin versus its cross-sectional area (Nield et al. 2004), has a significant effect on how streamlines are distorted (Bhattacharyya et al. 2006). These factors influence the degree of flow around a permeable cylinder; however, these studies only provided theoretical considerations of flow interception and the factors controlling the proportion of interception of permeable cylinders placed in open channels.

Most notably, the interception of flow through the porous cylinder was investigated analytically and numerically by Shahsavari et al. (2014). The most important case of this investigation was for conditions where a cylinder was laterally unbounded by flow in a channel. At PFM deployment sites in this study, this is the case, as the distance between the PFM and the channel bank is much larger than the PFM diameter. In these cases, the interception proportion, η, approaches zero when the Reynolds number, Re_D, of flow through the device, which is based on the length scale of the pore space of the material inside the cylinder, is less than 1.0. In other words, when Re_D is closer to the Re of the stream, interception is higher and the sampler more efficiently captures flowlines from the stream. Figure 4.1 displays the modeled relationship using a formula developed by Shahsavari et al. (2014) between Re_D, Da, and η for a range of values that are reasonable for the GAC and resin used as porous materials in this study. Using the grain size of the resin and the GAC, permeability (k, in m^2) and Darcy number were estimated (Freeze et al. 1979) (Table 2.5). The conditions for optimal interception of flow through a permeable cylinder

like the device that I designed for this study are quite limited and would require large or loosely packed granular material (i.e., higher Da and Re_D). The PFM likely had low permeabilities and low device Reynolds numbers, and as such, did not intercept a significant proportion of flow through the device during the deployment in the surface water. Interception of the PFM would also vary with streamflow conditions, as Re_D varies significantly with porous media properties and specific discharge through the device. As the subsurface water had much lower Reynolds numbers, the interception efficiency of the PFMs would likely be much larger than for the surface water PFMs.

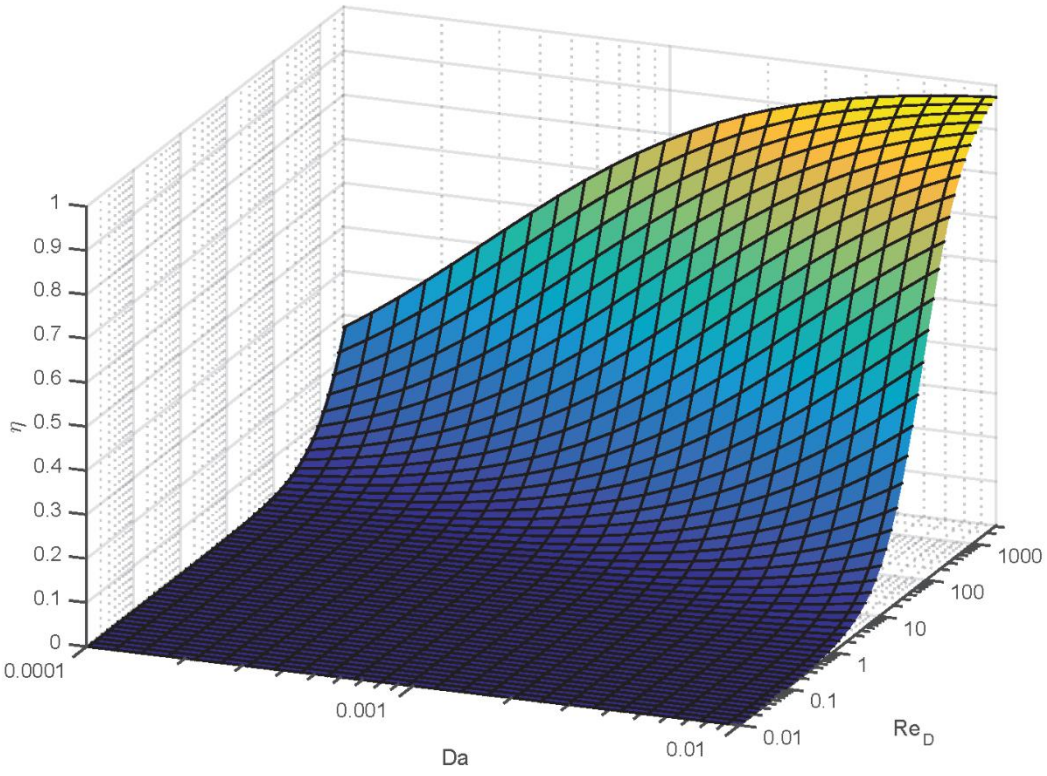

Figure 4.1. Interception efficiency, η, as a function of Darcy number and Reynolds number through the device. Darcy number $Da\left[\frac{k}{d^2}\right]$ is a measure of permeability of the porous media, and Reynolds number Re_D [-] represents the turbulence of water inside the device. The z axis (vertical axis) represents the interception efficiency (η), or the proportion of flow through the device relative to flow around the device.

Table 2.5. Approximate permeability, mean grain diameter, and Darcy number of PFM layer sorbent material (Freeze et al. 1979).

Media	Permeability, k (cm^2)	Grain diameter, d (cm)	Darcy number, Da (unitless)
Resin	10^{-6}	0.07	2×10^{-4}
GAC	10^{-5}	0.1	1×10^{-3}

4.5. Implications of low interception on cumulative discharge through the PFM

Poor interception of flow would have consequences on the discharge through the PFM and may have been the primary factor in the difference between surface water and subsurface water PFM cumulative discharge estimates. In the surface water, where interception may be much lower than in the subsurface, a greater proportion of streamlines move around the sampler due to the high velocity in the stream. In the subsurface water, laminar flow conditions are likely dominant and thus interception would be higher than in the surface water. The cumulative discharge estimated through the PFM was much more variable than the solute load on the PFM resins across all deployments, potentially due to variability in site-specific ambient stream conditions.

In addition, error in concentration estimates can be introduced via poor estimates of discharge based on the alcohol tracer method. The method of quantifying alcohol concentrations in solution using the GC can introduce laboratory error due to volatilization of the alcohols from improper handling or due to improper standard preparation. In addition, each tracer provides a different estimate of discharge due to differences in alcohol mass retained in the PFM after a deployment.

The estimate of cumulative discharge through the PFM was determined using an average of the estimates from each individual tracer remaining on the PFM after deployment. For most

deployments with higher estimated discharge and higher stream velocity, MeOH and EtOH eluted completely from the GAC, leaving only IPA and tBA within the range of viable M_R values to estimate discharge. As shown by Figure 3.4, each tracer estimate contained inherent variability in discharge estimates through the PFMs. If MeOH and EtOH were used to estimate the mean, these tracers tended to underestimate cumulative discharge through the PFM. Estimates using IPA and tBA together reduce the variability in cumulative discharge estimation.

4.6. Future research and recommendations

To strengthen the relationship between ambient stream velocity and PFM estimations, in addition to improving the relationship between estimated concentrations by the PFM and estimated concentrations using stream samples, I suggest modifications to PFM design, deployment constraints, and additional validation techniques. Changes to PFM methods used in this study have the potential to increase the likelihood of successful PFM deployments and decrease the variability in discharge and concentration estimates by the PFM.

First, the design should introduce far less drag in a stream of high ambient velocity. If a cylindrical PFM is oriented along the streamline direction, the surface area of contact between the PFM sorbents and the water would stay constant and not depend on streamline orientation. For a cylindrical PFM deployed vertically, the turbulent flowlines within the stream can enter the screened PFM in any orientation, potentially invalidating the assumption that streamlines are parallel within the device. In addition, orientation of the PFM along the stream direction provides the ability for the device to be deployed in stream water that is shallower than our applications. This design also provides the ability for the PFM to be loaded with additional sorbent to control the hydraulic conductivity inside the device (Sassman 2014). In order to increase hydraulic

conductivity in the device, gravel may be added as a separate layer to induce flow through the device and reduce losses in interception efficiency (Sassman 2014).

Reducing the deployment time may also improve the success of the PFM. Shorter deployment times increase the likelihood of a larger number of tracers being present on the device at the end of the PFM deployment, allowing more estimations of discharge via more tracers. In addition, shorter deployments make it easier to collect grab samples at a higher temporal resolution to calculate mean concentrations that are closer to true conditions. Other studies of surface water PFMs have constrained deployments down to hours or a few days (Klammler et al. 2007, Padowski et al. 2009, Sassman 2014). A shorter deployment time coupled with a design and orientation that increases interception efficiency has the potential to increase the accuracy of the PFM method in surface water.

These improvements to PFM implementation have the potential to minimize uncertainty in estimates made by the device and increase the relatability to site-specific stream conditions.

5.0. Conclusion

Monitoring forested headwater catchments and their tributaries is important to uncover the spatial and temporal variation in chemistry that exists in these systems. Monitoring of stream chemistry in remote areas with cost effective approaches is necessary for providing improved inventories of headwater regions and for potential water quality compliance in locations that are not part of monitoring networks. Passive flux meters (PFMs) have shown promise in providing point estimates of water flux and chemical load in groundwater, surface water, and hyporheic zones. In this study, a cylindrical slotted pipe PFM design was deployed in dilute headwater streams at the Hubbard Brook Experimental Forest over six week-long deployments. The efficacy of the PFM to characterize water flux and mean concentration of these streams was tested against grab sample concentrations and measured flows. Estimates of mean solute concentrations were similar to grab samples during high flow conditions in streams and for subsurface conditions in the streambed sediments. The performance of the PFMs for estimating concentration was worse during low flows. These results indicate that the design used was inadequate for our stream sites. The inconsistent performance of the PFM was likely due to flow divergence around the PFM sampler, as well as inherent variability in tracer dynamics and validation measurements. Results from this study suggest that sampler designs that have less influence on flow field dynamics will be necessary for future use of PFMs in streams or open channel systems that experience variable discharge and flow velocities.

References

Abbott, B. W., G. Gruau, J. P. Zarnetske, F. Moatar, L. Barbe, Z. Thomas, O. Fovet, T. Kolbe, S. Gu and A. C. Pierson-Wickmann (2018). "Unexpected spatial stability of water chemistry in headwater stream networks." Ecology letters **21**(2): 296-308.

Acuña, V., T. Datry, J. Marshall, D. Barceló, C. Dahm, A. Ginebreda, G. McGregor, S. Sabater, K. Tockner and M. Palmer (2014). "Why should we care about temporary waterways?" Science **343**(6175): 1080-1081.

Alexander, R. B., E. W. Boyer, R. A. Smith, G. E. Schwarz and R. B. Moore (2007). "The role of headwater streams in downstream water quality." Journal of the American Water Resources Association **43**(1): 41-59.

Annable, M. D., K. Hatfield, J. Cho, H. Klammler, B. L. Parker, J. A. Cherry and P. S. C. Rao (2005). "Field-scale evaluation of the passive flux meter for simultaneous measurement of groundwater and contaminant fluxes." Environmental Science & Technology **39**(18): 7194-7201.

Bailey, A. S., J. W. Hornbeck, J. L. Campbell and C. Eagar (2003). Hydrometeorological database for Hubbard Brook Experimental Forest: 1955-2000, US Department of Agriculture, Forest Service, Northeastern Research Station Newtown Square.

Bailey, S. W., P. A. Brousseau, K. J. McGuire and D. S. Ross (2014). "Influence of landscape position and transient water table on soil development and carbon distribution in a steep, headwater catchment." Geoderma **226**: 279-289.

Basu, N. B., P. S. C. Rao, I. C. Poyer, M. D. Annable and K. Hatfield (2006). "Flux-based assessment at a manufacturing site contaminated with trichloroethylene." Journal of Contaminant Hydrology **86**(1-2): 105-127.

Benstead, J. P. and D. S. Leigh (2012). "An expanded role for river networks." Nature Geoscience **5**(10): 678.

Bernhardt, E. S., G. E. Likens, D. C. Buso and C. T. Driscoll (2003). "In-stream uptake dampens effects of major forest disturbance on watershed nitrogen export." Proceedings of the National Academy of Sciences of the United States of America **100**(18): 10304-10308.

Bhattacharyya, S., S. Dhinakaran and A. Khalili (2006). "Fluid motion around and through a porous cylinder." Chemical Engineering Science **61**(13): 4451-4461.

Bishop, K., I. Buffam, M. Erlandsson, J. Folster, H. Laudon, J. Seibert and J. Temnerud (2008). "Aqua Incognita: the unknown headwaters." Hydrological Processes **22**(8): 1239-1242.

Bryant, M. D., T. Gomi and J. J. Piccolo (2007). "Structures Linking Physical and Biological Processes in Headwater Streams of the Maybeso Watershed, Southeast Alaska." Forest Science **53**(2): 371-383.

Buso, D. C., G. E. Likens and J. S. Eaton (2000). "Chemistry of precipitation, streamwater, and lakewater from the Hubbard Brook Ecosystem Study: a record of sampling protocols and analytical procedures."

Cho, J. Y., M. D. Annable, J. W. Jawitz and K. Hatfield (2007). "Passive flux meter measurement of water and nutrient flux in saturated porous media: Bench-scale laboratory tests." Journal of Environmental Quality **36**(5): 1266-1272.

Clark, G. M., D. K. Mueller and M. A. Mast (2000). "Nutrient concentrations and yields in undeveloped stream basins of the United States." JAWRA Journal of the American Water Resources Association **36**(4): 849-860.

Clinton, B. D. and J. M. Vose (2006). "Variation in Stream Water Quality in an Urban Headwater Stream in the Southern Appalachians." Water, Air, and Soil Pollution **169**(1): 331-353.

Crawford, J. T., L. C. Loken, N. J. Casson, C. Smith, A. G. Stone and L. A. Winslow (2015). "High-Speed Limnology: Using Advanced Sensors to Investigate Spatial Variability in Biogeochemistry and Hydrology." Environmental Science & Technology **49**(1): 442-450.

Creed, I. F., D. M. McKnight, B. A. Pellerin, M. B. Green, B. A. Bergamaschi, G. R. Aiken, D. A. Burns, S. E. Findlay, J. B. Shanley and R. G. Striegl (2015). "The river as a chemostat: fresh perspectives on dissolved organic matter flowing down the river continuum." Canadian Journal of Fisheries and Aquatic Sciences **72**(8): 1272-1285.

Detty, J. M. and K. J. McGuire (2010). "Topographic controls on shallow groundwater dynamics: implications of hydrologic connectivity between hillslopes and riparian zones in a till mantled catchment." Hydrological Processes **24**(16): 2222-2236.

Dodds, W. K. and R. M. Oakes (2008). "Headwater influences on downstream water quality." Environmental Management **41**(3): 367-377.

Downing, J. A., J. J. Cole, C. M. Duarte, J. J. Middelburg, J. M. Melack, Y. T. Prairie, P. Kortelainen, R. G. Striegl, W. H. McDowell and L. J. Tranvik (2012). "Global abundance and size distribution of streams and rivers." Inland Waters **2**(4): 229-236.

Driscoll, C. T. and G. E. Likens (1982). "Hydrogen-Ion Budget of an Aggrading Forested Ecosystem." Tellus **34**(3): 283-292.

Driscoll, C. T., G. E. Likens, L. O. Hedin, J. S. Eaton and F. H. Bormann (1989). "Changes in the chemistry of surface waters." Environmental Science & Technology **23**(2): 137-143.

Elmore, A. J., J. P. Julian, S. M. Guinn and M. C. Fitzpatrick (2013). "Potential stream density in Mid-Atlantic US watersheds." PLoS One **8**(8): e74819.

Ensign, S. H. and M. W. Doyle (2006). "Nutrient spiraling in streams and river networks." Journal of Geophysical Research-Biogeosciences **111**(G4).

Fenn, M. E. and M. A. Poth (2004). "Monitoring nitrogen deposition in throughfall using ion exchange resin columns: A field test in the San Bernardino Mountains." Journal of Environmental Quality **33**(6): 2007-2014.

Findlay, S. (1995). "Importance of surface-subsurface exchange in stream ecosystems: The hyporheic zone." Limnology and oceanography **40**(1): 159-164.

Freeze, R. A. and J. A. Cherry (1979). Groundwater, Prentice-Hall.

Fritz, K. M., E. Hagenbuch, E. D'Amico, M. Reif, P. J. Wigington, S. G. Leibowitz, R. L. Comeleo, J. L. Ebersole and T. L. Nadeau (2013). "Comparing the extent and permanence of headwater streams from two field surveys to values from hydrographic databases and maps." JAWRA Journal of the American Water Resources Association **49**(4): 867-882.

Gannon, J. P., S. W. Bailey, K. J. McGuire and J. B. Shanley (2015). "Flushing of distal hillslopes as an alternative source of stream dissolved organic carbon in a headwater catchment." Water Resources Research **51**(10): 8114-8128.

Gillin, C. P., S. W. Bailey, K. J. McGuire and J. P. Gannon (2015). "Mapping of Hydropedologic Spatial Patterns in a Steep Headwater Catchment." Soil Science Society of America Journal **79**(2): 440-453.

Godsey, S. E., J. W. Kirchner and D. W. Clow (2009). "Concentration–discharge relationships reflect chemostatic characteristics of US catchments." Hydrological Processes **23**(13): 1844-1864.

Hall Jr, R., E. S. Bernhardt and G. E. Likens (2002). "Relating nutrient uptake with transient storage in forested mountain streams." Limnology and Oceanography **47**(1): 255-265.

Hatfield, K., M. Annable, J. H. Cho, P. S. C. Rao and H. Klammler (2004). "A direct passive method for measuring water and contaminant fluxes in porous media." Journal of Contaminant Hydrology **75**(3-4): 155-181.

Herlihy, A. T., J. L. Stoddard and C. B. Johnson (1998). "The relationship between stream chemistry and watershed land cover data in the mid-Atlantic region, US." Water, Air, and Soil Pollution **105**(1-2): 377-386.

Hill, A. R. and D. J. Lymburner (1998). "Hyporheic zone chemistry and stream-subsurface exchange in two groundwater-fed streams." Canadian Journal of Fisheries and Aquatic Sciences **55**(2): 495-506.

Hunsaker, C. T. and D. W. Johnson (2017). "Concentration-discharge relationships in headwater streams of the Sierra Nevada, California." Water Resources Research **53**(9): 7869-7884.

Johnson, A. H. (1979). "Estimating solute transport in streams from grab samples." Water Resources Research **15**(5): 1224-1228.

Johnson, C. E., J. J. Ruiz-Méndez and G. B. Lawrence (2000). "Forest Soil Chemistry and Terrain Attributes in a Catskills Watershed." Soil Science Society of America Journal **64**: 1804-1814.

Johnson, N. M., C. T. Driscoll, J. S. Eaton, G. E. Likens and W. H. Mcdowell (1981). "Acid-Rain, Dissolved Aluminum and Chemical-Weathering at the Hubbard-Brook

Experimental Forest, New-Hampshire." Geochimica Et Cosmochimica Acta **45**(9): 1421-1437.

Kirchner, J. W., X. H. Feng, C. Neal and A. J. Robson (2004). "The fine structure of water-quality dynamics: the (high-frequency) wave of the future." Hydrological Processes **18**(7): 1353-1359.

Kjonaas, O. J. (1999). "In situ efficiency of ion exchange resins in studies of nitrogen transformation." Soil Science Society of America Journal **63**(2): 399-409.

Klaminder, J., R. Bindler, H. Laudon, K. Bishop, O. Emteryd and I. Renberg (2006). "Flux rates of atmospheric lead pollution within soils of a small catchment in northern Sweden and their implications for future stream water quality." Environmental Science & Technology **40**(15): 4639-4645.

Klammler, H., M. A. Newman, E. Szilagyi, J. C. Padowski, K. Hatfield, J. W. Jawitz and M. D. Annable (2007). "Initial test results for a passive surface water fluxmeter to measure cumulative water and solute mass fluxes." Environmental Science & Technology **41**(7): 2485-2490.

Kolberg, R. L., B. Rouppet, D. G. Westfall and G. A. Peterson (1997). "Evaluation of an in situ net soil nitrogen mineralization method in dryland agroecosystems." Soil Science Society of America Journal **61**(2): 504-508.

Krause, S., J. Lewandowski, C. N. Dahm and K. Tockner (2015). "Frontiers in real-time ecohydrology - a paradigm shift in understanding complex environmental systems." Ecohydrology **8**(4): 529-537.

Kunz, J. V., M. D. Annable, J. Cho, W. von Tumpling, K. Hatfield, S. Rao, D. Borchardt and M. Rode (2017). "Quantifying nutrient fluxes with a new hyporheic passive flux meter (HPFM)." Biogeosciences **14**(3): 631-649.

Langlois, J. L., D. W. Johnson and G. R. Mehuys (2003). "Adsorption and Recovery of Dissolved Organic Phosphorus and Nitrogen by Mixed-Bed Ion-Exchange Resin." Soil Science Society of America Journal **67**: 889-894.

Langlois, J. L., D. W. Johnson and G. R. Mehuys (2003). "Adsorption and recovery of dissolved organic phosphorus and nitrogen by mixed-bed ion-exchange resin." Soil Science Society of America Journal **67**(3): 889-894.

Lawrence, G. B. and C. T. Driscoll (1990). "Longitudinal Patterns of Concentration Discharge Relationships in Stream Water Draining the Hubbard-Brook-Experimental-Forest, New-Hampshire." Journal of Hydrology **116**(1-4): 147-165.

Lawrence, G. B., R. D. Fuller and C. T. Driscoll (1986). "Spatial Relationships of Aluminum Chemistry in the Streams of the Hubbard Brook Experimental Forest, New-Hampshire." Biogeochemistry **2**(2): 115-135.

Likens, G. E. (2013). Biogeochemistry of a forested ecosystem, Springer Science & Business Media.

Likens, G. E. (2017). "Fifty years of continuous precipitation and stream chemistry data from the Hubbard Brook ecosystem study (1963–2013)." Ecology **98**(8): 2224-2224.

Likens, G. E. and D. C. Buso (2006). "Variation in streamwater chemistry throughout the Hubbard Brook Valley." Biogeochemistry **78**(1): 1-30.

Likens, G. E. and D. C. Buso (2012). "Dilution and the elusive baseline." Environmental science & technology **46**(8): 4382-4387.

Likens, G. E., C. T. Driscoll, D. C. Buso, M. J. Mitchell, G. M. Lovett, S. W. Bailey, T. G. Siccama, W. A. Reiners and C. Alewell (2002). "The biogeochemistry of sulfur at Hubbard Brook." Biogeochemistry **60**(3): 235-316.

Likens, G. E., C. T. Driscoll, D. C. Buso, T. G. Siccama, C. E. Johnson, G. M. Lovett, T. J. Fahey, W. A. Reiners, D. F. Ryan, C. W. Martin and S. W. Bailey (1998). "The biogeochemistry of calcium at Hubbard Brook." Biogeochemistry **41**(2): 89-173.

Lowe, W. H. and G. E. Likens (2005). "Moving headwater streams to the head of the class." BioScience **55**(3): 196-197.

McGuire, K. J., C. E. Torgersen, G. E. Likens, D. C. Buso, W. H. Lowe and S. W. Bailey (2014). "Network analysis reveals multiscale controls on streamwater chemistry." Proceedings of the National Academy of Sciences **111**(19): 7030-7035.

Mulholland, P. J. (1992). "Regulation of Nutrient Concentrations in a Temperate Forest Stream - Roles of Upland, Riparian, and Instream Processes." Limnology and Oceanography **37**(7): 1512-1526.

Musolff, A., C. Schmidt, B. Selle and J. H. Fleckenstein (2015). "Catchment controls on solute export." Advances in Water Resources **86**: 133-146.

Neal, C., B. Reynolds, P. Rowland, D. Norris, J. W. Kirchner, M. Neal, D. Sleep, A. Lawlor, C. Woods, S. Thacker, H. Guyatt, C. Vincent, K. Hockenhull, H. Wickham, S. Harman and L. Armstrong (2012). "High-frequency water quality time series in precipitation and streamflow: From fragmentary signals to scientific challenge." Science of the Total Environment **434**: 3-12.

Nield, D. A., A. V. Kuznetsov and M. Xiong (2004). "Effects of Viscous Dissipation and Flow Work on Forced Convection in a Channel Filled by a Saturated Porous Medium." Transport in Porous Media **56**(3): 351-367.

Padowski, J. C., E. A. Rothfus, J. W. Jawitz, H. Klammler, K. Hatfield and M. D. Annable (2009). "Effect of Passive Surface Water Flux Meter Design on Water and Solute Mass Flux Estimates." Journal of Hydrologic Engineering **14**(12): 1334-1342.

Palmer, S. M. and C. T. Driscoll (2002). "Decline in mobilization of toxic aluminium." Nature **417**: 242.

Palmer, S. M., C. T. Driscoll and C. E. Johnson (2004). "Long-term trends in soil solution and stream water chemistry at the Hubbard Brook Experimental Forest: relationship with landscape position." Biogeochemistry **68**(1): 51-70.

Palmer, S. M., B. I. Wellington, C. E. Johnson and C. T. Driscoll (2005). "Landscape influences on aluminium and dissolved organic carbon in streams draining the Hubbard Brook valley, New Hampshire, USA." Hydrological Processes **19**(9): 1751-1769.

Pinar, E., G. M. Ozkan, T. Durhasan, M. M. Aksoy, H. Akilli and B. Sahin (2015). "Flow structure around perforated cylinders in shallow water." Journal of Fluids and Structures **55**: 52-63.

Rode, M., A. J. Wade, M. J. Cohen, R. T. Hensley, M. J. Bowes, J. W. Kirchner, G. B. Arhonditsis, P. Jordan, B. Kronvang, S. J. Halliday, R. A. Skeffington, J. C. Rozemeijer, A. H. Aubert, K. Rinke and S. Jomaa (2016). "Sensors in the Stream: The High-Frequency Wave of the Present." Environmental Science & Technology **50**(19): 10297-10307.

Ross, D. S., J. B. Shanley, J. L. Campbell, G. B. Lawrence, S. W. Bailey, G. E. Likens, B. C. Wemple, G. Fredriksen and A. E. Jamison (2012). "Spatial patterns of soil nitrification and nitrate export from forested headwaters in the northeastern United States." Journal of Geophysical Research-Biogeosciences **117**.

Rozemeijer, J., Y. Van Der Velde, H. de Jonge, F. van Geer, H.-P. Broers and M. Bierkens (2010). "Application and evaluation of a new passive sampler for measuring average solute concentrations in a catchment scale water quality monitoring study." Environmental science & technology **44**(4): 1353-1359.

Sanford, S. E., I. F. Creed, C. L. Tague, F. D. Beall and J. M. Buttle (2007). "Scale-dependence of natural variability of flow regimes in a forested landscape." Water Resources Research **43**(8).

Sassman, S. A. (2014). A new passive surface water flux meter for simultaneous measurement of contaminant and water fluxes in streams and rivers, Purdue University.

Shahsavari, S., B. L. Wardle and G. H. McKinley (2014). "Interception efficiency in two-dimensional flow past confined porous cylinders." Chemical Engineering Science **116**: 752-762.

Susfalk, R. B. and D. W. Johnson (2002). "Ion exchange resin based soil solution lysimeters and snowmelt solution collectors." Communications in Soil Science and Plant Analysis **33**(7-8): 1261-1275.

Swistock, B. R., P. J. Edwards, F. Wood and D. R. Dewalle (1997). "Comparison of methods for calculating annual solute exports from six forested Appalachian watersheds." Hydrological Processes **11**(7): 655-669.

Temnerud, J. and K. Bishop (2005). "Spatial Variation of Streamwater Chemistry in Two Swedish Boreal Catchments: Implications for Environmental Assessment." Environmental Science & Technology **39**(6): 1463-1469.

Tiwari, T., I. Buffam, R. A. Sponseller and H. Laudon (2017). "Inferring scale-dependent processes influencing stream water biogeochemistry from headwater to sea." Limnology and Oceanography **62**(S1).

Tritton, D. J. (2012). Physical fluid dynamics, Springer Science & Business Media.

Verreydt, G., M. D. Annable, S. Kaskassian, I. Van Keer, J. Bronders, L. Diels and P. Vanderauwera (2013). "Field demonstration and evaluation of the Passive Flux Meter on a CAH groundwater plume." Environmental Science and Pollution Research **20**(7): 4621-4634.

Watmough, S. A., J. Aherne, C. Alewell, P. Arp, S. Bailey, T. Clair, P. Dillon, L. Duchesne, C. Eimers and I. Fernandez (2005). "Sulphate, nitrogen and base cation budgets at 21 forested catchments in Canada, the United States and Europe." Environmental Monitoring and Assessment **109**(1-3): 1-36.

Wohl, E. (2017). "The significance of small streams." Frontiers of Earth Science **11**(3): 447-456.

Wolock, D. M., J. Fan and G. B. Lawrence (1997). "Effects of basin size on low-flow stream chemistry and subsurface contact time in the Neversink River Watershed, New York." Hydrological Processes **11**(9): 1273-1286.

Yang, J. E., E. O. Skogley, S. J. Georgitis, B. E. Schaff and A. H. Ferguson (1991). "Phytoavailability Soil Test: Development and Verification of Theory." Soil Science Society of America Journal **55**: 1358-1365.

Yu, P., Y. Zeng, T. S. Lee, X. B. Chen and H. T. Low (2011). "Steady flow around and through a permeable circular cylinder." Computers & Fluids **42**(1): 1-12.

Zimmer, M. A., S. W. Bailey, K. J. McGuire and T. D. Bullen (2013). "Fine scale variations of surface water chemistry in an ephemeral to perennial drainage network." Hydrological Processes **27**(24): 3438-3451.

Appendices

A. GC-FID method

The method for the GC-FID was set as follows: the initial temperature was 45 °C, held for 6 minutes, ramped up at 3 °C per minute to 75 °C, held for 3 minutes, ramped up at 10 °C per minute to 130 °C, then ramped up at 30 °C per minute to 240 °C. The FID temperature was held at 240 °C. Hydrogen gas flow was 40 mL per minute, and air flow was 450 mL per minute. The Helium gas pressure was 4 psi. The injection volume was 1 μL. The syringe was washed 3 times before and after each sample injection, and each sample was pumped 3 times before injection into the column. The split ratio of the GC was 1:10 for all samples. 9 mixed standards were prepared to create calibration curves for MeOH, EtOH, IPA, tBA, and DMP. Calibration curves are provided in Figure A-1. A chromatogram for one PFM initial sample (**A**) and two PFM final samples (**B** and **C**) are provided in Figure A-2.

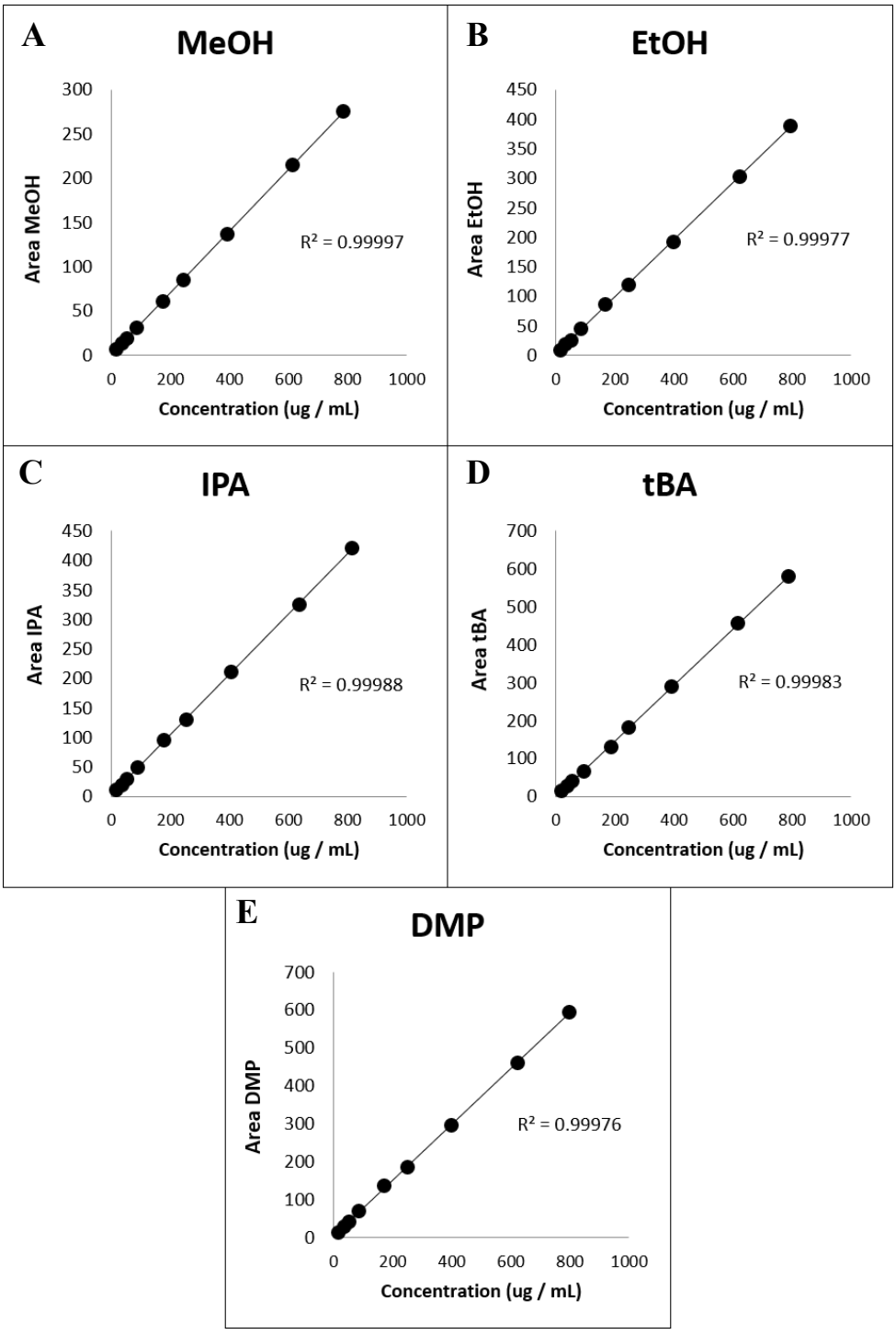

Figure A-1. Calibration curves for MeOH (**A**), EtOH (**B**), IPA (**C**), tBA (**D**), and DMP (**E**) for GC – FID analysis. The y-axis represents peak area under the curve for instrument response for each chromatogram.

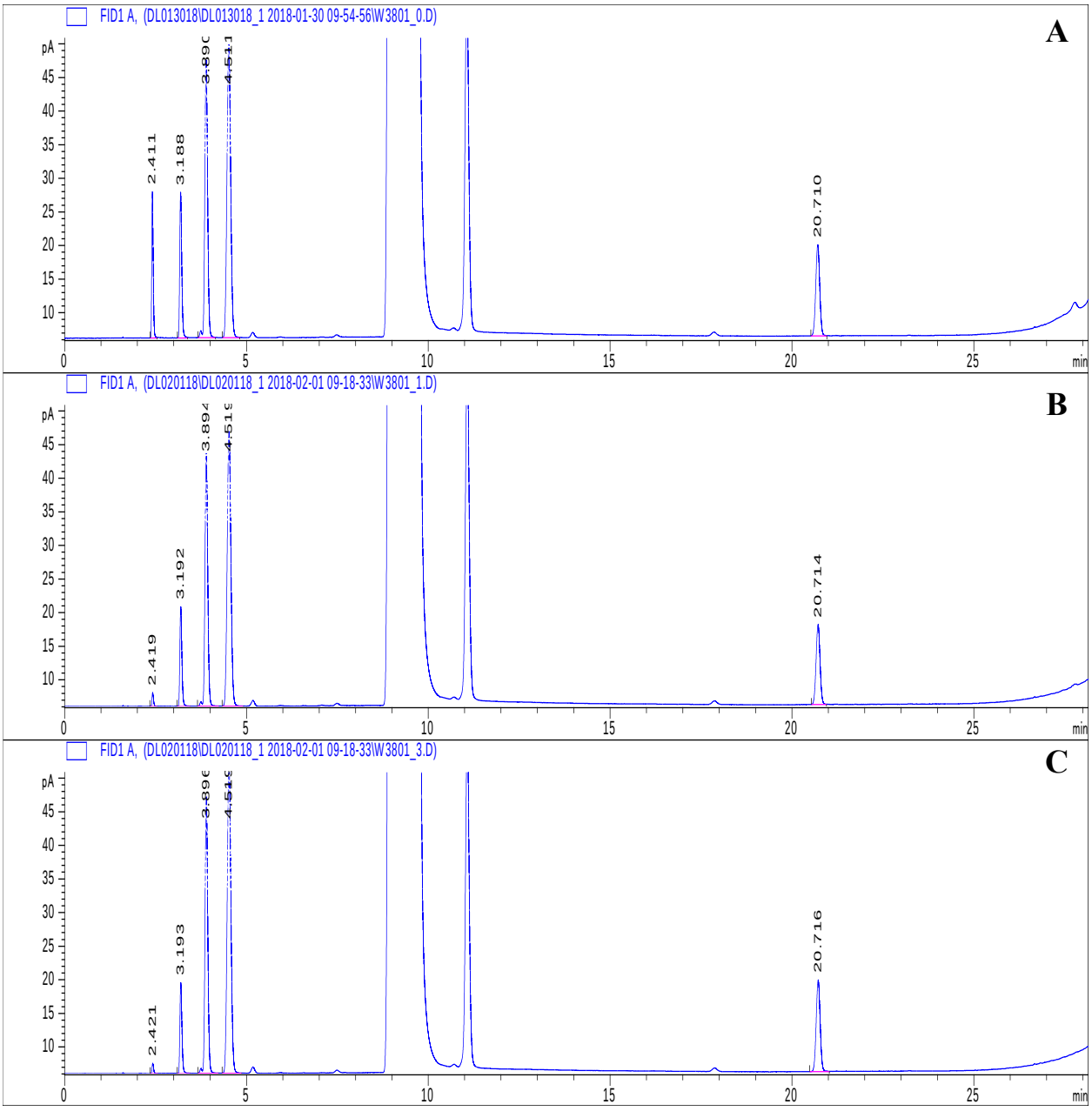

Figure A-2. Chromatogram for W3 PFM, 8/01/17 deployment. Chromatograms present for an initial (**A**), final top layer (**B**), and final bottom layer (**C**) sample of GAC. Peaks in order and corresponding retention times are (from left to right): MeOH (2.4 min), EtOH (3.2 min), IPA (3.9 min), tBA (4.5 min), IBOH (9-10 min), secondary IBOH (11 min), and DMP (20.7 min).

B. PFM Darcy flux vs. PFM cumulative discharge.

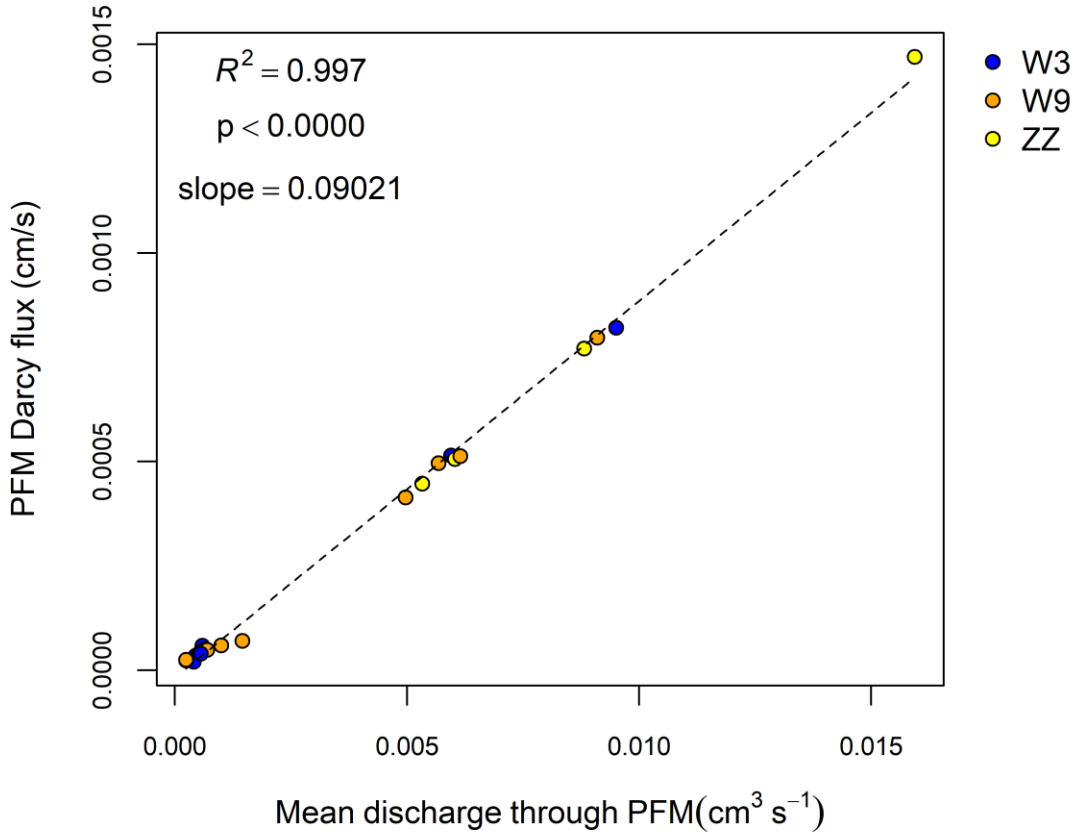

Figure B-1. Different expressions of flow through the PFM. Darcy flux was determined using Eqn. 2.1 and volume through the PFM was determined using Eqn. 2.6.